5-2011

Characteristics of the Fields in the Near and Far Zone Of Antennas and Its Significance in Wireless Communication

Arijit De
Syracuse University

CHARACTERISTICS OF THE FIELDS IN THE NEAR AND THE FAR ZONE OF ANTENNAS AND ITS SIGNIFICANCE IN WIRELESS COMMUNICATION

By

Arijit De

BTech (Hons.), Indian Institute of Technology, Kharagpur, India 2004

DISSERTATION

Submitted in partial fulfillment of the requirements for the degree of Doctor of Philosophy in Electrical Engineering in the Graduate School of Syracuse University.

May 2011

Advisor: Prof. Tapan K. Sarkar

Co-Advisor: Prof. Magdalena Salazar-Palma

Abstract

The characterization of the fields radiated from antennas in wireless communication scenario has been mostly overlooked by communication society. The definition and application of Near-Field and Far-field has mostly been considered from the antenna measurement community. To date no critical study does exist for the evaluation of the far-field criterion in a wireless communication scenario. This dissertation tries to provide certain guidelines characterizing the near-field and the far-field using a Maxwellian framework. The implications of the near-field environment are then discussed. It appears that the concept of near and far fields are not clearly interpreted in the wireless communication literature. This dissertation tries to provide some insight into the trade-off of the phenomenon of height-gain and the near field zone of the antenna which determines the optimum positioning of the transmitting antenna within a cellular range.

Acknowledgements

The author is very much indebted to his research advisors Prof. Tapan K. Sarkar and Prof. Magdalena Salazar-Palma for their keen interest and expert guidance throughout the course of this work. Their extensive knowledge and vast experience has been a major asset and source of inspiration for the author at every stage of this work.

The author would like to extend his appreciation to Prof Jay K. Lee and Prof. Ercument Arvas for spending their precious time during many hours of discussions which resulted in very fruitful suggestions; and to, Prof. Qi Wang Song, Prof. Carlos Hartmann, and Prof. Ashok S. Sangani for serving as a member of the examining committee. The author would also like to thank Dr. Mary C. Taylor for serving as the reader of the dissertation.

Finally the author expresses his heart-felt gratitude to the members of CEMLAB, Syracuse University, and to the family and friends for providing their personal support at various times.

Table of Contents

1. INTRODUCTION

The commonly used characterization as given in classical books of antennas like Kraus and Marhefka [2002], of the transition of the near-field to the far-field of an antenna is $2 D^2 / \lambda$, where λ is the wave-length corresponding to the free space and D is the maximum overall dimension of the antenna. The goal here is to demonstrate the variation of the different characteristics and the properties of the field radiated by the antenna commonly encountered in a wireless communication scenario. From these characteristics we might be able to determine the distance at which the far-field characteristics of the field tend to appear and hence we can have a fair judgment of the position of the Transmitter and Receiver.

The most widely used antenna in most of the systems is a dipole antenna. Although radiation from a dipole antenna is pretty well-established, not much of the study has been done regarding the near-field and the far-field due to a dipole antenna placed above a ground plane, which typically arises in a wireless communication environment. In Sarkar, Micks et. al. [2003] and Sarkar et. al. [2006] the authors emphasize the need for incorporation of the electromagnetic principles for an efficient system design using a Maxwellian framework. Sarkar et. al. [2008] and Sarkar, Palma and Mokole [2008] discusses the concept of channel capacity in the near-field region of the antenna, when the power is complex number and demonstrates that Hartley based Channel capacity is more suitable than Shannon based form. Thus the characterization of the near-field to far-field transition assumes immense significance in the wireless communication application.

In this dissertation we have chosen few criteria to differentiate the near-field from the

far-field. In the far-field of an antenna the field component along the radial direction is quite low compared to the field component that is desired to be received which is perpendicular to the radial component (like the θ-component for a dipole oriented vertically along the z-direction or the Φ-component for the horizontally oriented dipole). This Field transversality criterion of choosing the far-field can be set as the distance where the radial component is lower than the desired component by a factor of 40dB or 60dB.

The second widely used argument for the characterization of the far-field is the distance where the real part of the wave impedance approaches the free-space wave impedance i.e. η_o (which is numerically equal to 120π) and the phase of the wave impedance approaches 0. The wave impedance is determined by ratio of the desired E-field (i.e. θ-component for a vertically oriented dipole antenna above the ground plane or the Φ-component for the horizontally oriented dipole antenna above the ground plane) to the corresponding desired H-field (i.e. φ-component for a vertically oriented dipole antenna above the ground plane or the θ -component for the horizontally oriented dipole antenna above the ground plane). Closely associated with it is the criterion based on the power density being real in the far-field. In other words the Poynting vector (E x H*) is a complex number in the near-zone of the antenna with sufficiently large imaginary portion, while in the far-zone of the antenna the Poynting vector is a real number.

The third criterion that can be used to distinguish the near-field from the far-field is based on the constant 1/r decay of the field in the radiating far-zone of the antenna. Though there is no unique characterization of the behavior of the source in the near zone, but in the radiation zone the field generally falls off in amplitude by 1/r. The boundary

between the near-field and the far-field region is vaguely defined. It is dependent on the dominant wavelength emitted by the source. Different people use different terminologies. Some people define near-field region (or rather near zone) as the region within a radius $r \ll \lambda$, while the far-field region (or rather far zone or radiation zone) as the region for which $r \gg \lambda$. The two regions are defined simply for mathematical convenience to obtain certain simplifying approximations. Here we study all of the above criteria for both the vertical and the horizontally oriented half-wave dipole antenna above ground plane.

2. ANTENNAS ABOVE PERFECTLY ELECTRICALLY CONDUCTING (PEC) GROUND

2.1 Introduction

We first consider a half-wave center fed dipole antenna operating at a frequency of 1 GHz, over a PEC ground plane. The simulation setup is shown in Figure 1 below. The center of the transmitting dipole antenna is located H_t above the PEC ground plane. The observation point for the near-field is located H_r above the PEC ground plane. The horizontal distance between the Transmitting antenna and the observation point is D. This is the most commonly occurring scenario in wireless communication. What we are interested is the variation of the field and some of it's characteristics (like the real part of the impedance and its phase), as we move away from the transmitting antenna i.e. as we increase D. We are interested in the θ-component and the radial component of the electric field as is shown in Figure 1 below.

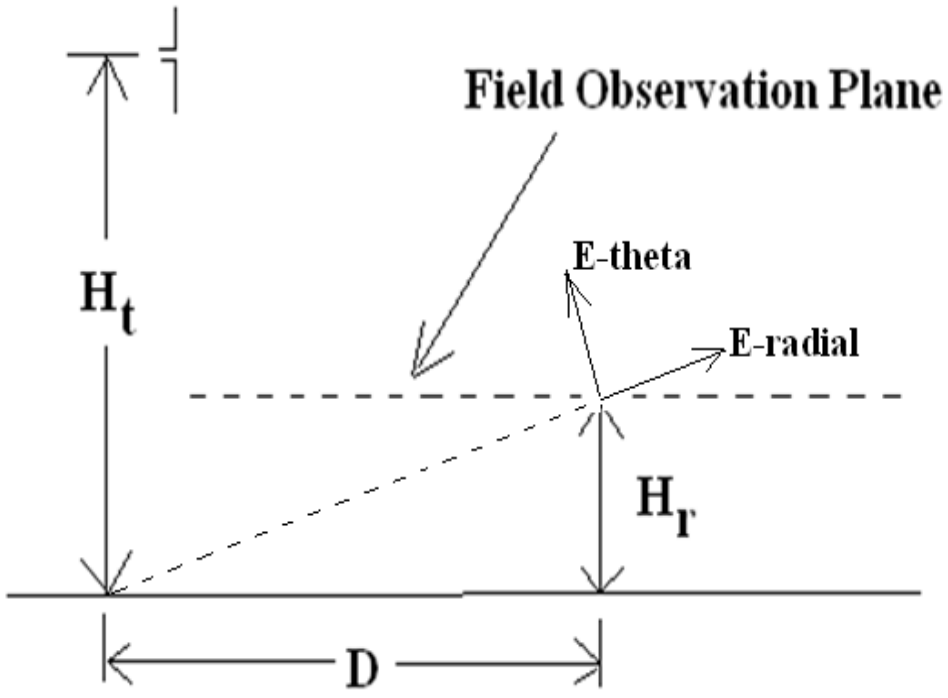

Figure 1: Schematic of the simulation setup.

2.2 Vertical Dipole above PEC Ground

2.2.1 Co-Polar Component of the radiated field

We first consider the vertical dipole antenna above the PEC ground. The variation of the magnitude of the θ-component of the Electric field along with D is shown in Figure 2 below. The blue broken line shows the magnitude of E_θ when the transmitting dipole antenna is located at a height 0.25m above the PEC ground. The observation of the field is at a height 2.0m above the PEC ground. We can see that there is a null at 1.0m and another null at 6.67m. After 12.5m the field decays as 1/r. So after 12.5 m we can claim that the receiver is in the far-field of the transmitter. But as we bring the transmitting dipole higher up to 2.0m keeping the observation height the same as 2.0m above PEC ground, we observe something significantly different as shown in the red dotted line of Figure 2 below. We see that the variation of the magnitude of the field with distance has more wild variation with increasing number of nulls and peaks. This is what is commonly referred to in the communication literature as large scale fading [4]. The last null now occurs at 50m from the transmitter. Thus after around 100m from the receiver the field decays regularly as 1/r as one would observe when the observation receiver is in the far-field of the transmitting antenna. This clearly indicates that the higher the transmitter antenna is positioned above the ground plane, the further is the distance where the far-field zone of the receiver antenna begins. This is more evident from the third graph as shown by green solid line in Figure 2. The transmitter is now placed at a height of 10.0m from the PEC ground. The variation of the magnitude of the field with distance is now more rapidly oscillating, with the last null being at 250m. The roll-off with 1/r follows

after a distance of 500m from the transmitter.

Thus we can draw some conclusions from the above discussions. As we bring the antenna above the ground (in this case PEC) we see the distance where the field exhibits the far-field behavior is at a larger distance compared to the case when the transmitting antenna is located closer to the ground. It also appears from the above figures that the approximate distance at which the far-field phenomenon exhibits in the form of constant roll-of at 1/r, changes linearly with the height of the transmitting antenna above the ground.

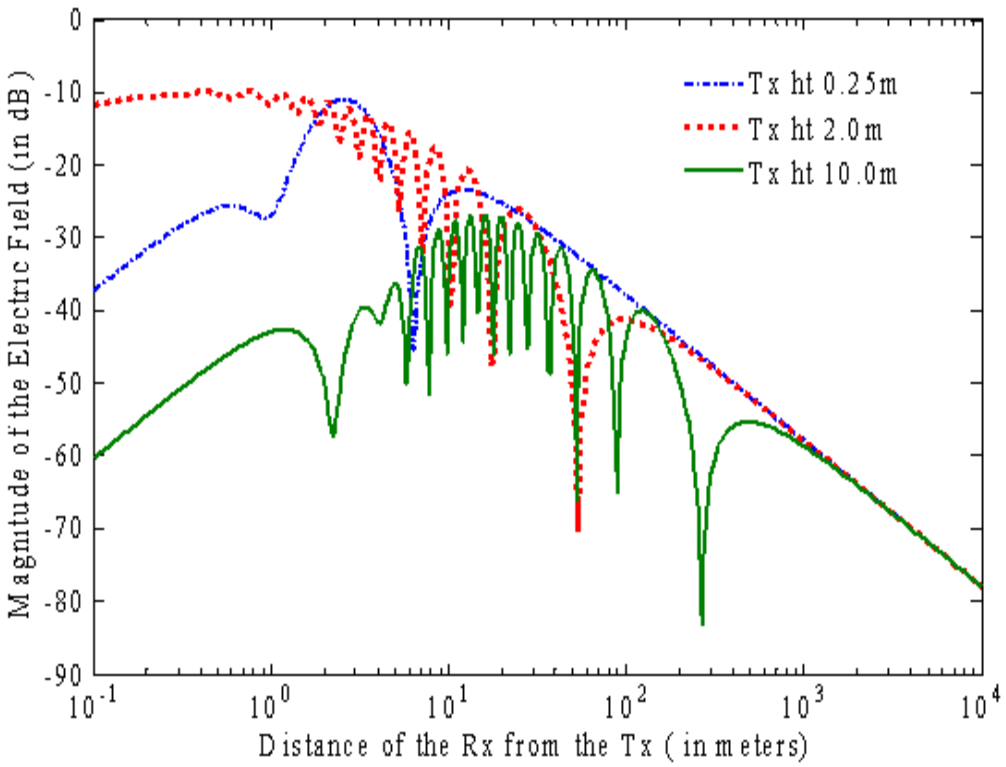

Figure 2: The magnitude of the theta component due to a vertically oriented transmitting dipole antenna above the PEC ground plane for different transmitter

heights. The observation of the field is at a height of 2m from the PEC ground plane.

2.2.2 Cross-Polar Component of the radiated field

Figure 3 below shows the magnitude of the radial component of the electric field as described in the schematic in Figure 1. Ideally, the radial component is not desired in the far zone of the antenna and it should decay as fast as $1/r^3$, with distance. The blue broken line in Figure 3 below shows the radial component when the transmitter is located at a height of 0.25m. It can be seen that there is less oscillation with the last null of the magnitude of the radial component of the field being at 3.35m and the field decays as $1/r^3$ after a distance of 6.67m. The red dotted line corresponds to the transmitter height of 2.0m while the observation points are located at the same height of 2.0m. We observe that there is more oscillation with distance than the previous case when the transmitting antenna was closer to the ground. The last null of the magnitude of the radial component appears at 25m and the field decays as $1/r^3$ after a distance of 50m. As the transmitting antenna is brought further higher above the PEC ground to 10.0m (which is indicated by green solid lines in Figure 3 below), the field oscillates more rapidly as in the case of the theta component of the field as discussed before. The last null appears at 125m from the transmitting antenna and the field shows the far-field behavior i.e. roll-off at $1/r^3$ after a distance of 250m.

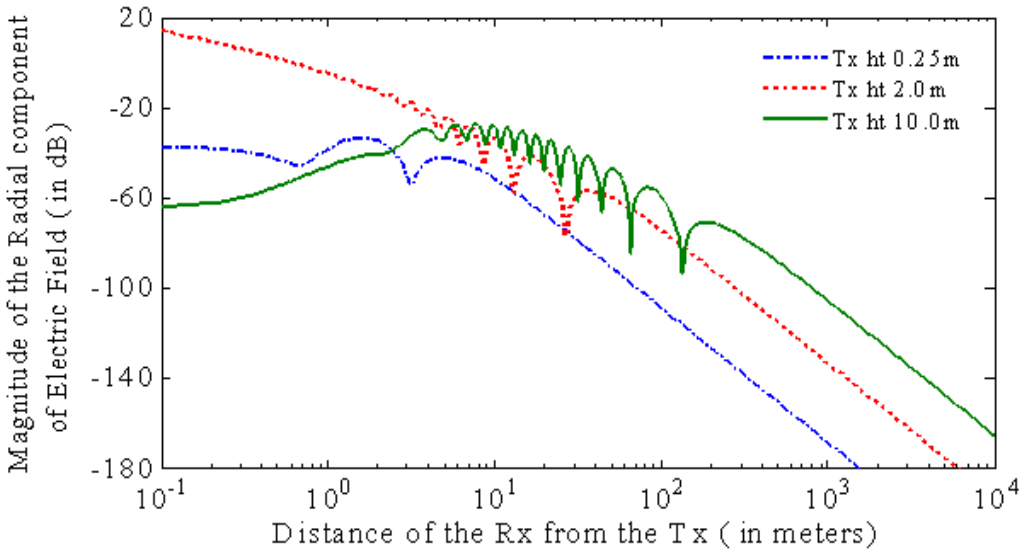

Figure 3: The magnitude of the radial component of the electric field due to a vertically oriented transmitting dipole antenna above the PEC ground plane for different transmitter heights. The observation of the field is at a height of 2m from the PEC ground plane.

Even for the case of the radial component of the electric field we can draw similar conclusions as we discussed for the theta component. As the antenna is brought higher up above the ground plane, there is more rapid variation of the field with distance, going through alternate peaks and nulls. The location of the last null (or the location of the last peak after which the field decays as $1/r^3$), increases linearly with the height of the transmitting antenna above ground plane. In the far-field it is desirable to have the radial component of the electric field to be as small as possible. This means the sooner it starts decaying as $1/r^3$ the closer the far-field zone of the antenna starts. Thus the closer the antenna is to the ground plane the closer the far-field zone of the antenna starts. This in

turn ensures that the receiver is less likely to fall in such large scale fading or other kinds of complex near-field scenario.

Another thing worth noticing from Figure 3 is the fact that as the transmitting antenna is brought higher above the ground plane, the radial field component increases in the far-field for a constant input power fed at the input of the antenna. As observed from Figure 2, the theta component of the field is almost the same in the far-field zone for various heights of the transmitting antenna above the ground plane. This once again leads us to a conclusion that the transmitting antenna should be placed closer to the ground in order for the far-field zone to start closer to the transmitter and also to have reduced radial component.

Comparing Figure 2 with Figure 3 we can conclude that the radial component of the field decays as $1/r^3$ (as it should do in the far-field zone of the antenna) at almost half the distance from the transmitter compared to the case where the theta component of the electric field i.e. E_θ exhibits the far-field behavior. This can also be observed from Figure 4 below where the red solid lines indicate the theta component of the electric field as defined in the schematic in Figure 1. The blue broken line indicates the radial component of the electric field. The transmitting antenna in this case is located 5.0m above PEC ground, while the receiving observation points are located 2.0m above the ground. As can be seen from Figure 4, the radial component is lower than the theta component of the electric field by a factor of 60dB at a distance of almost 1Km. It should be noted that the typical cell size in a cellular based wireless communication varies around 1~3 Km. The base station transmitting antennas are normally placed at least on a 10-20m tall tower. Thus within the entire region of the cell size, the radial component is quite high compared

to the theta component. It seems that the operation of the cellular communications in this scenario is mostly in the near-field regime. On the other hand, if we bring the antenna closer to the ground then this distance at which the radial component is lower than the theta component by -60dB, is reduced to 200m. We again see that the distance scales linearly with the height of the transmitting antenna above the PEC ground. This is used as an alternate criterion for choosing the far field condition provided the theta component and the radial component of the electric field decays as 1/r and $1/r^3$ respectively.

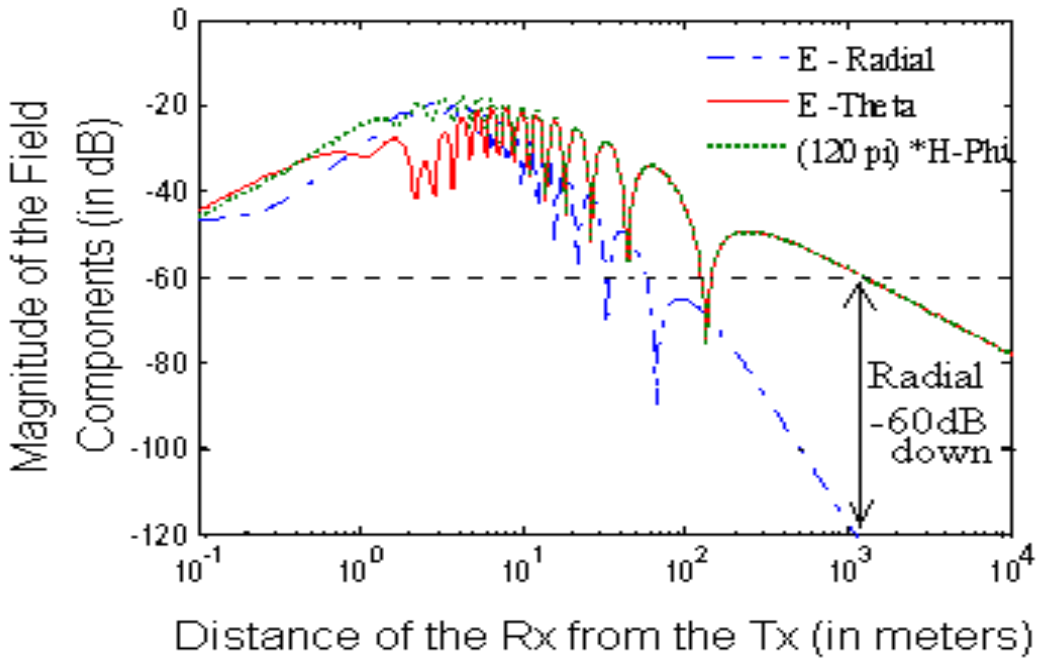

Figure 4: Theta component of E-Field, the Radial component of E-Field and the Phi component of H-Field multiplied by η (which is the impedance of the free space) when the Transmitter is 5.0m from the ground and the Receiver is 2.0m from the ground.

2.2.3 Wave Impedance of the radiated field

Impedance of the wave is another crucial criterion for the determination of the far zone of the antenna. The red solid line in Figure 4 above shows the θ-component of the electric field for the transmitter located at a height of 5.0m from the PEC ground and the receiving points located at a height of 2.0m from the PEC ground. The green dotted line shows the Φ-component of the magnetic field multiplied by η_0, where η_0 is the impedance of the free space which is numerically close to 120π. The impedance of the field is given by,

$$\eta = \frac{E_\theta}{H_\phi}.$$

Normally in the far-field region of the antenna, the ratio η is a real number and is equal to η_0. But in the near field region of the antenna, η is generally a complex number. Comparing the red solid line and the green dotted line we see that there is considerable difference between them up to a distance of around 10m. After 10m the curves agree each other very well. This implies that η differs considerably from η_0 up to 10m distance after which they are close to each other. But at least it seems from the figure that the rapid oscillation with the presence of nulls and peaks are still present even though the impedance has converged to η_0.

The variation of the real part of the impedance (η) with distance is shown in Figure 5 below. The solid blue curve corresponds to the case when the transmitter antenna is placed 2.0m above PEC ground but the observation point is fixed at 2.0m from the ground. The real part of the impedance approaches η_0 at around 10m while the 1/r roll-off

in the far field regime starts at around 100m. As the transmitting antenna is brought higher up to 5.0m from the ground (as shown in the red broken line), the distance at which the real part of the impedance approaches η_0 is around 25m. However the distance at which the 1/r roll-off in the far field occurs is close to 250m which is almost 10 times higher than the distance obtained considering the real part of the impedance. The dotted green line in Figure 5 shows the real part of the impedance when the transmitter is located at 10m from the ground. The real part of the impedance in this case approaches η_0 at a distance of 50m.

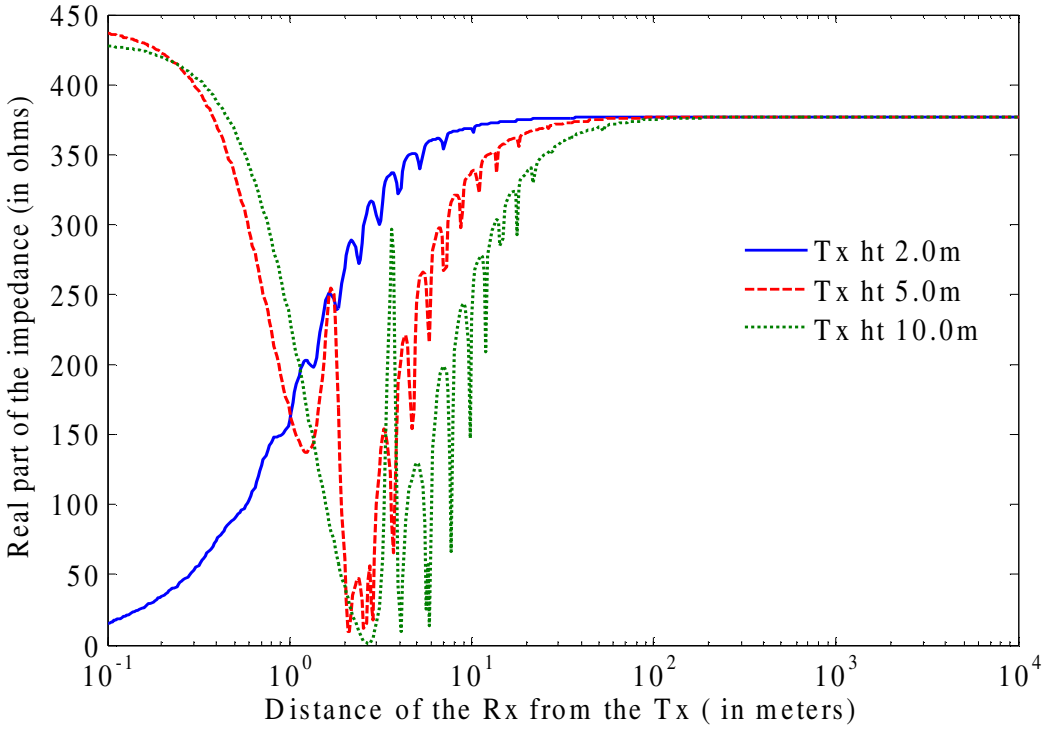

Figure 5: Variation of the real part of the wave impedance with the distance, for different transmitter heights of the vertically oriented dipole antenna above the PEC

ground plane.

The far-field E_θ and H_Φ are in phase with each other. In other words, the phase angle of the impedance of the wave (i.e. η) should be close to zero in the far-field region of the antenna. Figure 6 below shows the variation of the phase angle of the impedance with distance of the observation point from the receiver, for various heights of the transmitting antenna.

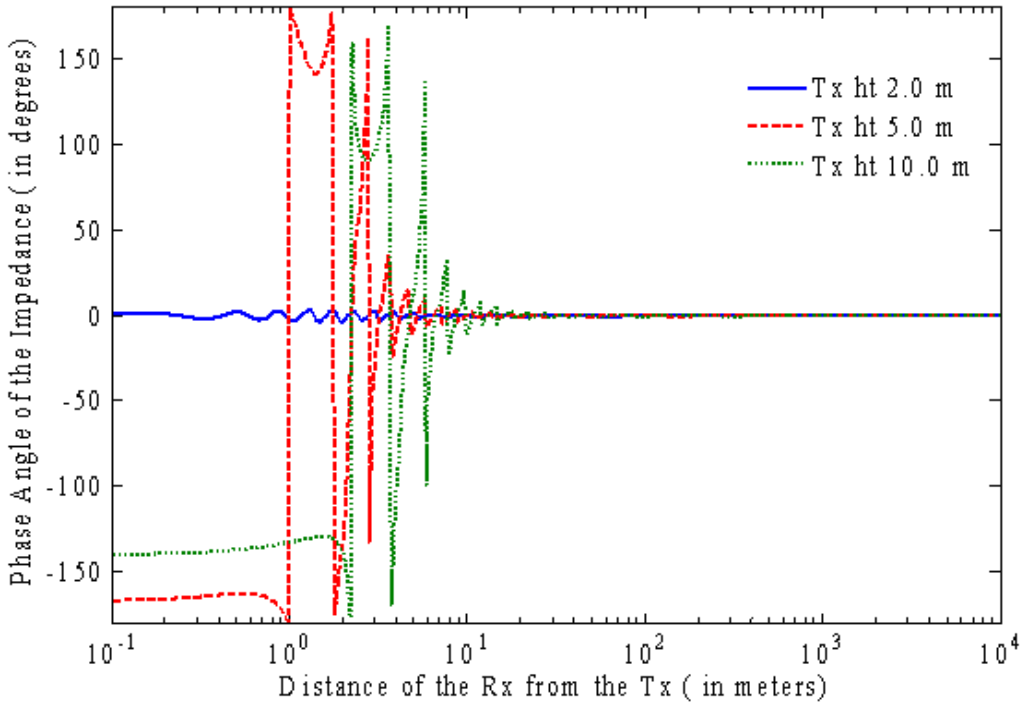

Figure 6: Variation of the phase angle of the wave impedance with the distance, for different transmitter heights of the vertically oriented dipole antenna above the PEC ground plane.

The blue solid line shows the phase variation for transmitter located at 2m above PEC. The phase is almost very close to zero as should be desired in the far-zone of the antenna. As the transmitting antenna is moved higher up to 5.0m above PEC, (as shown in the broken red line) the phase angle varies widely and then converges to zero at a distance which is smaller than the distance at which the real part of the impedance approaches η_0. Similar is the case for the height of the transmitting antenna when it is placed 10m above PEC ground as shown by the dotted green line. The phase angle approaches zero at around 20m which is smaller than the distance at which the real part of the impedance converges.

Figure 7 below shows the variation of real part of the impedance (η) in blue solid line with distance of the observation point from the transmitting antenna and the transmitting antenna located at 10m above the PEC ground, while the green dotted line shows the variation of the magnitude of the theta component of the electric field with distance.

It is clear from the figures that the impedance is not a strict condition on the far field criterion. It determines the transition of the very near-field zone to the near-field zone of the antenna. The sphericity condition i.e. the decay of the field strength as 1/r is a more appropriate characterization to determine the transition of the near-field and the far-field region of the transmitting antenna above a PEC ground plane .

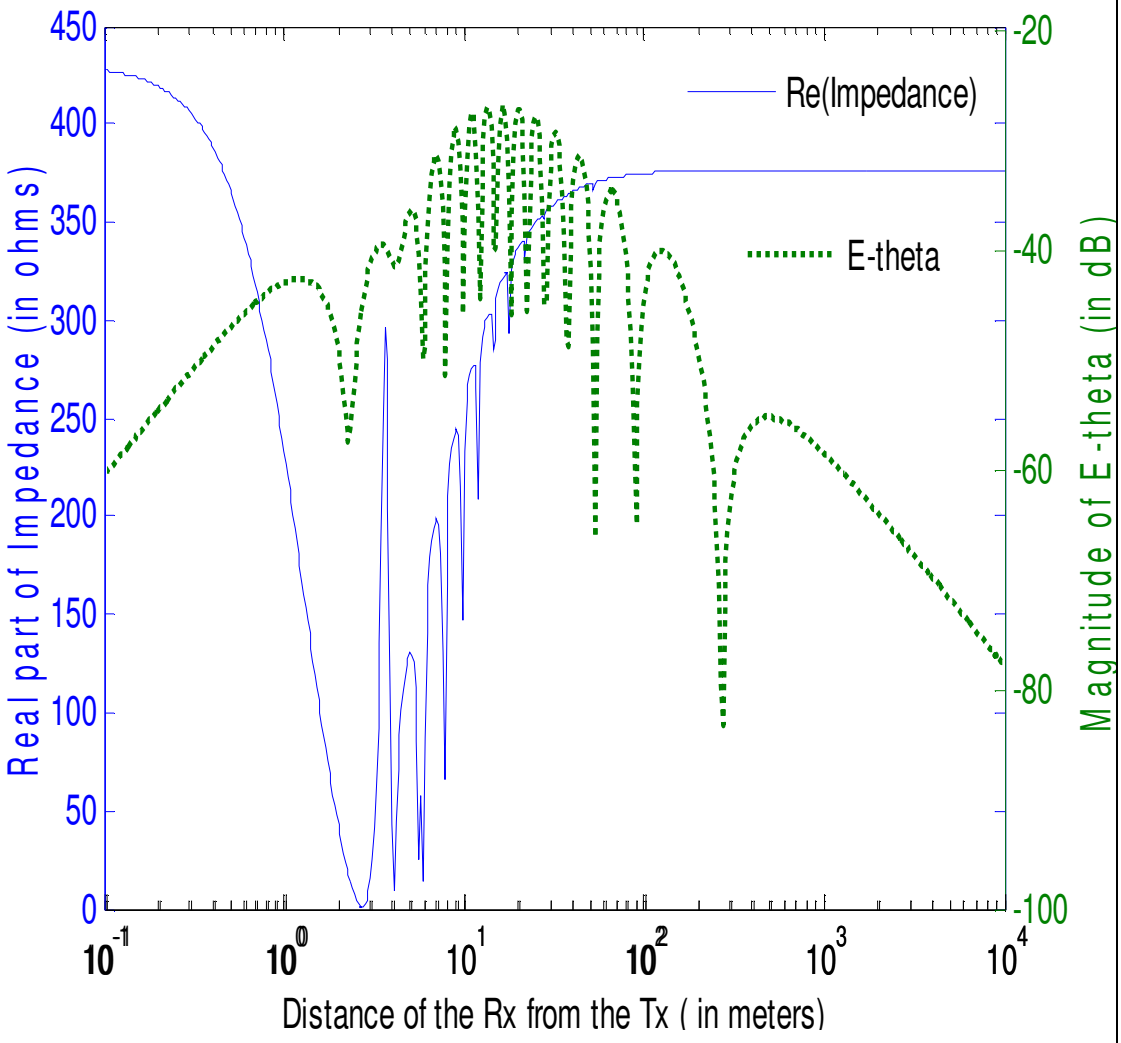

Figure 7: Comparison of the near-field to far-field transition due to wave impedance and the wave sphericity condition of the theta component of the Electric field decaying by 1/R for the vertically oriented dipole antenna above PEC ground plane.

2.2.4 Field components when the height of the receiver is varied

It is of some interest to observe how the field variation changes when the observation height changes, keeping the transmitter antenna at the fixed position as before. The blue broken line in Figure 8 indicates the magnitude of the theta component of the field when the observation is located at a height of 0.5m. The last null is located at a distance of 66.67m from the transmitter. As we change the observation height to 1.0m as shown by the red dotted line, the last null shifts further to 133.34m. The green solid line has the observation location at a height of 2.0m from the PEC ground plane. The last null in this case shifts further to 266.67m from the transmitter.

We observe from the above discussion that as the vertically oriented transmitting antenna is moved higher above the PEC ground plane, the field varies more rapidly with the appearance of the increased number of nulls and peaks due to the contribution of the image source. The position at which the far-field starts appearing based on different criterion, goes further away as the height of the vertically oriented transmitter is placed higher up above the ground plane. Several different criteria have been used to characterize the location of the boundary between the near-field and the far-field. The results using the above criterion are discussed below.

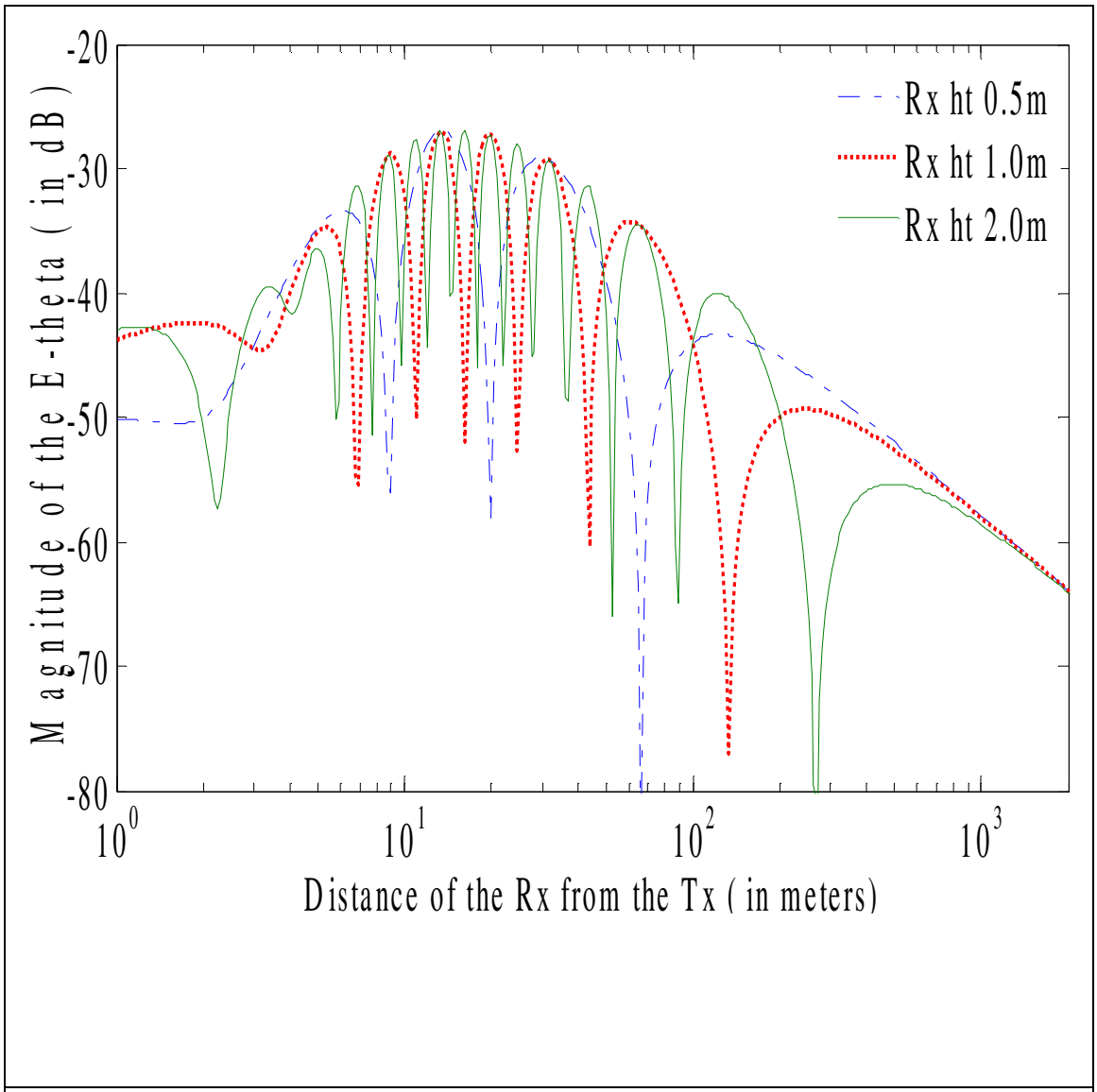

Figure 8: Variation of the theta component of the Electric field with distance from the transmitter for various heights of the receiver for the field observation.

2.2.5 Analysis of the Radiated Field

The theta component and the radial component of the Electric Field due to a Hertzian dipole in free space is given by,

$$E_\theta = \eta Idl \sin\theta \frac{e^{-j\beta r}}{4\pi r}\left(j\beta + \frac{1}{r} + \frac{1}{j\beta r^2} \right) \tag{1}$$

$$E_r = \eta Idl \cos\theta \frac{e^{-j\beta r}}{4\pi r}\left(\frac{2}{r} + \frac{2}{j\beta r^2} \right) \tag{2}$$

By transformation of coordinate from polar to Cartesian the Electric field is given by,

$$\begin{aligned} E_z &= -E_\theta \sin\theta + E_r \cos\theta \\ &= \eta Idl \frac{e^{-j\beta r}}{4\pi r}\left[-\sin^2\theta \left(j\beta + \frac{1}{r} + \frac{1}{j\beta r^2} \right) + \cos^2\theta \left(\frac{2}{r} + \frac{2}{j\beta r^2} \right) \right] \end{aligned} \tag{3}$$

$$\begin{aligned} E_x &= E_\theta \cos\theta + E_r \sin\theta \\ &= \eta Idl \frac{e^{-j\beta r}}{4\pi r} \cos\theta \sin\theta \left[\left(j\beta + \frac{1}{r} + \frac{1}{j\beta r^2} \right) + \left(\frac{2}{r} + \frac{2}{j\beta r^2} \right) \right] \end{aligned} \tag{4}$$

In order to calculate the field due to a Hertzian dipole placed vertically above the PEC, using image theory the PEC can be replaced by two vertically oriented dipole (A and B) in the same direction as shown in the Figure 9 below. The total field due to both the dipoles is given by,

$$\begin{aligned} E_z &= E_{z_1}(\theta_1) + E_{z_2}(\theta_2) \\ E_x &= E_{x_1}(\theta_1) + E_{x_2}(\theta_2) \end{aligned} \tag{5}$$

The theta component of the Electric field due to both the dipoles is given by,

$$E_\theta = E_z \sin\theta - E_x \cos\theta \tag{6}$$

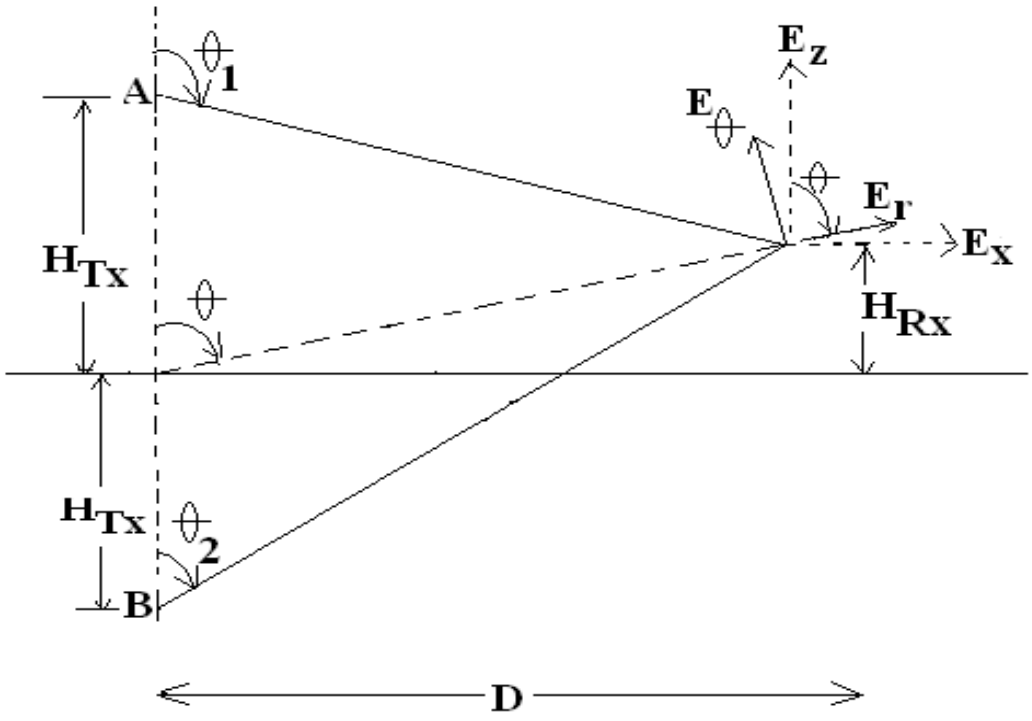

Figure 9: Two Hertzian dipole using the image theory and its various field components.

For D » H_{Tx} and D » H_{Rx}, we can approximate $\theta \rightarrow \pi/2$, $\theta_1 \rightarrow \pi/2$, and $\theta_2 \rightarrow \pi/2$. Using Eq. 1, the theta component of the Electric Field due to the vertically oriented dipole antenna can be approximated as,

$$E_\theta = -\eta Idl \left[\frac{e^{-j\beta r_1}}{4\pi r_1} \left(j\beta + \frac{1}{r_1} + \frac{1}{j\beta r_1^2} \right) + \frac{e^{-j\beta r_2}}{4\pi r_2} \left(j\beta + \frac{1}{r_2} + \frac{1}{j\beta r_2^2} \right) \right] \tag{7}$$

For distance r » λ/2π, i.e., for distance further than the very reactive near-field of the antenna, the contribution due to where the contribution due to 1/r and $1/r^2$ terms are negligible. We can thus approximate the theta component of the Electric field as,

$$E_\theta = -j\beta\eta Idl\left[\frac{e^{-j\beta r_1}}{4\pi r_1}+\frac{e^{-j\beta r_2}}{4\pi r_2}\right] \tag{8}$$

where r_1 and r_2 are given by,

$$r_1=\sqrt{(H_{Tx}-H_{Rx})^2+D^2} \tag{9}$$

$$r_2=\sqrt{(H_{Tx}+H_{Rx})^2+D^2} \tag{10}$$

For large distances of D compared to H_{Tx} and H_{Rx}, r_1 and r_2 can be approximated as,

$$\begin{aligned} r_1 &= \sqrt{(H_{Tx}-H_{Rx})^2+D^2} \\ &= D\sqrt{1+\frac{(H_{Tx}-H_{Rx})^2}{D^2}} \\ &\approx D\left(1+\frac{1}{2}\frac{(H_{Tx}-H_{Rx})^2}{D^2}\right) \end{aligned} \tag{11}$$

and

$$\begin{aligned} r_2 &= \sqrt{(H_{Tx}+H_{Rx})^2+D^2} \\ &= D\sqrt{1+\frac{(H_{Tx}+H_{Rx})^2}{D^2}} \\ &\approx D\left(1+\frac{1}{2}\frac{(H_{Tx}+H_{Rx})^2}{D^2}\right) \end{aligned} \tag{12}$$

Since the effect of the difference of the amplitude is not much, so one can assume the amplitude to be pretty much constant and, r_1 and r_2 can be approximated by D. On the

other hand the phase is more sensitive to the difference between r_1 and r_2. Based on these approximations, the theta component of the electric field given in Eq. 8 can be approximated as,

$$
\begin{aligned}
E_\theta &= -\, j\beta\eta Idl \left[\frac{e^{-j\beta r_1}}{4\pi r_1} + \frac{e^{-j\beta r_2}}{4\pi r_2} \right] \\
&\approx -\frac{j\beta\eta Idl}{4\pi D} \left[e^{\frac{-j2\pi r_1}{\lambda}} + e^{\frac{-j2\pi r_2}{\lambda}} \right] \\
&\approx -\frac{j\beta\eta Idl}{4\pi D} e^{\frac{-j2\pi D}{\lambda}} \left[e^{\frac{-j2\pi}{\lambda}\frac{\left(H_{Tx}-H_{Rx}\right)^2}{2D}} + e^{\frac{-j2\pi}{\lambda}\frac{\left(H_{Tx}+H_{Rx}\right)^2}{2D}} \right] \\
&= -\frac{j\beta\eta Idl}{4\pi D} e^{\frac{-j2\pi D}{\lambda}} e^{\frac{-j2\pi}{\lambda}\frac{\left(H_{Tx}^2+H_{Rx}^2\right)}{2D}} \left[e^{\frac{j2\pi}{\lambda}\frac{H_{Tx}H_{Rx}}{D}} + e^{\frac{-j2\pi}{\lambda}\frac{H_{Tx}H_{Rx}}{D}} \right] \\
&= -\frac{j\beta\eta Idl}{2\pi D} e^{\frac{-j2\pi D}{\lambda}} e^{\frac{-j2\pi}{\lambda}\frac{\left(H_{Tx}^2+H_{Rx}^2\right)}{2D}} \cos\frac{2\pi H_{Tx}H_{Rx}}{\lambda D}
\end{aligned}
\tag{13}
$$

Thus the magnitude of the theta component of the Electric field exhibits a sinusoid oscillation with deeps nulls and peaks. In the far-field the cosine term approaches unity and the magnitude of the field decays as 1/D as shown in Fig. 2, 4, 8. The distance D at which the theta-component of the Electric field goes to zero is given by,

$$
\begin{aligned}
&\cos\frac{2\pi H_{Tx}H_{Rx}}{\lambda D} = 0 \\
\Rightarrow\ &\frac{2\pi H_{Tx}H_{Rx}}{\lambda D} = \frac{\pi}{2} + m\pi \ , m \in \mathbf{I} \\
\Rightarrow\ &D = \frac{2H_{Tx}H_{Rx}}{\left(\frac{1}{2}+m\right)\lambda}
\end{aligned}
\tag{14}
$$

The position of the last null after which no further oscillations occur and once can claim that the Receiving antenna is in the far-field of the Transmitting antenna is given by m = 0. Thus the position of the last null is given by,

$$D = \frac{4H_{Tx}H_{Rx}}{\lambda} \tag{15}$$

The figure below provides the comparison of the theta component of the Electric field when the transmitting antenna is placed 10m above PEC ground and the observation point is located 2m above the PEC ground. The blue solid line indicates the field due to a radiating Hertzian dipole antenna for which explicit analytical expressions can be derived. The red broken line is due to a half-wavelength dipole antenna with its field shifted down along the Y-axis for the sake of comparison. Note that the nulls and the peaks do appear in the similar positions as in the case of the Hertzian dipole as the transmitting antenna. The green dotted line corresponds to the field due to approximate formulae given by Eq. 13. The formula is valid for the horizontal distance (D) between the Transmitter and the Receiver being much larger than the height of the Transmitter (H_{Tx}) and the Receiver (H_{Rx}) from the PEC ground plane. It can be seen from the Figure 10 below that for D>30m i.e. almost after $3H_{Tx}$, the field variation due to the approximate formulae given by the green dotted line agree quite well with the blue solid line , i.e. the exact field distribution due to a Hertzian dipole antenna. The last null is supposed to be as given by Eq. 15 and is at a distance of 266.67m from the Transmitter. The position of the some other nulls also agree with the formulae given by Eq. 14 , so

long as D is at least 3 times the Height of the Transmitter and the Height of the Receiver above the PEC ground plane. As can be seen from the figure below that the predicted position of the other nulls and the simulated with both the exact field due to a Hertzian dipole and due to a half-wavelength dipole antenna agree very well and are at the positions 29.63m, 53.33m, 88.89m, 266.67m. All the other nulls closer to the Transmitting antenna do not agree very well as the approximation made by Eq. 13 is not valid enough because the distance D is closer to the transmitting antenna compared to the height of the antenna above the PEC ground plane.

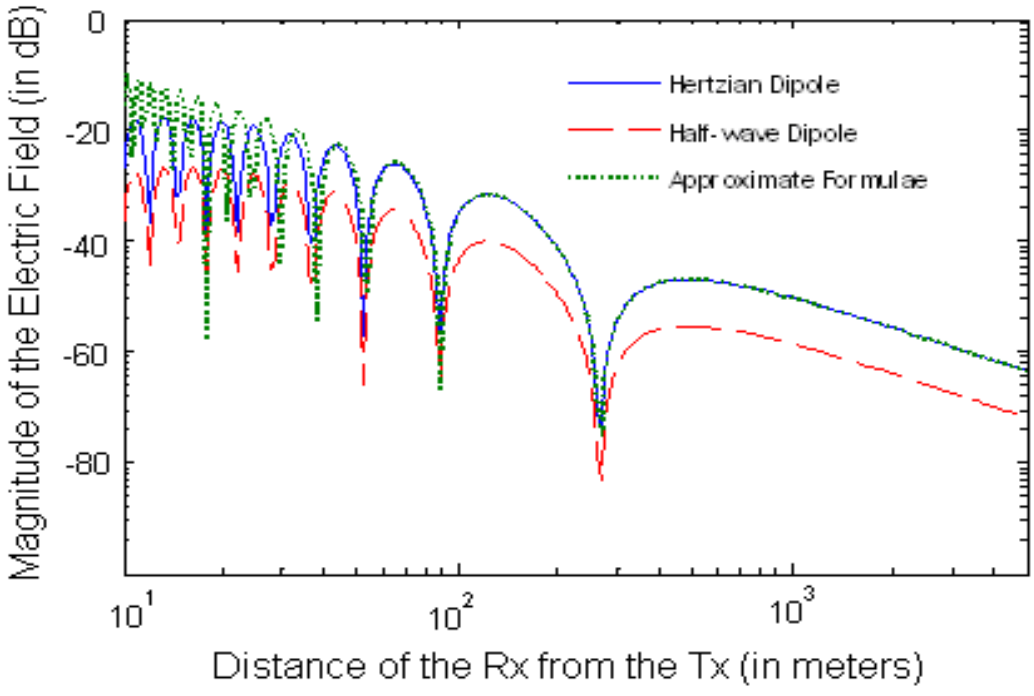

Figure 10: Comparison of the field behavior for the Hertzian dipole, half-wave dipole and the due to the approximate formulae given by Eq. 13 when the transmitting antenna is placed 10m above PEC ground and the field is observed 2m

above the ground.

Figure 11 below, summarizes the position of the last null for different heights of the vertically oriented half-wave transmitting dipole antenna above the PEC ground plane based on the simulation result using a full-wave electromagnetic simulator. The blue line with crosses indicates the position of the last null for the field observation height at 0.5m above the ground plane. The red line with squares, the green line with triangles and the black line with circles correspond to the field observation heights of 1.0m, 2.0m, and 3.0m respectively. It can be seen that the position of the last null changes linearly with the height of the transmitting antenna above the ground plane and all the lines in Fig. 11 below, agrees with the predicted formulae given by Eq. 15.

It is to be noted that after the last null, the magnitude of the theta component of the electric field again reaches a maximum after which it rolls-off as 1/r, which is the required far-field criterion. The distance at which the theta component of the electric field is within -3dB of the 1/r decay is given by the condition,

$$20\log\left(\cos\frac{2\pi H_{Tx}H_{Rx}}{\lambda D}\right)=-3$$

$$\Rightarrow \cos\frac{2\pi H_{Tx}H_{Rx}}{\lambda D}=\frac{1}{\sqrt{2}} \tag{16}$$

$$\Rightarrow D=\frac{8H_{Tx}H_{Rx}}{\lambda}$$

The position of the last maxima as given in Fig. 2, which determines the distance at which the far-field starts, is thus approximately given by,

$$\frac{\partial}{\partial D}\left(\frac{\cos\frac{2\pi H_{Tx}H_{Rx}}{\lambda D}}{D}\right)=0$$

$$\Rightarrow\frac{\frac{2\pi H_{Tx}H_{Rx}}{\lambda D}\sin\frac{2\pi H_{Tx}H_{Rx}}{\lambda D}-\cos\frac{2\pi H_{Tx}H_{Rx}}{\lambda D}}{D^2}=0 \qquad (17)$$

$$\Rightarrow\frac{2\pi H_{Tx}H_{Rx}}{\lambda D}\tan\frac{2\pi H_{Tx}H_{Rx}}{\lambda D}=1$$

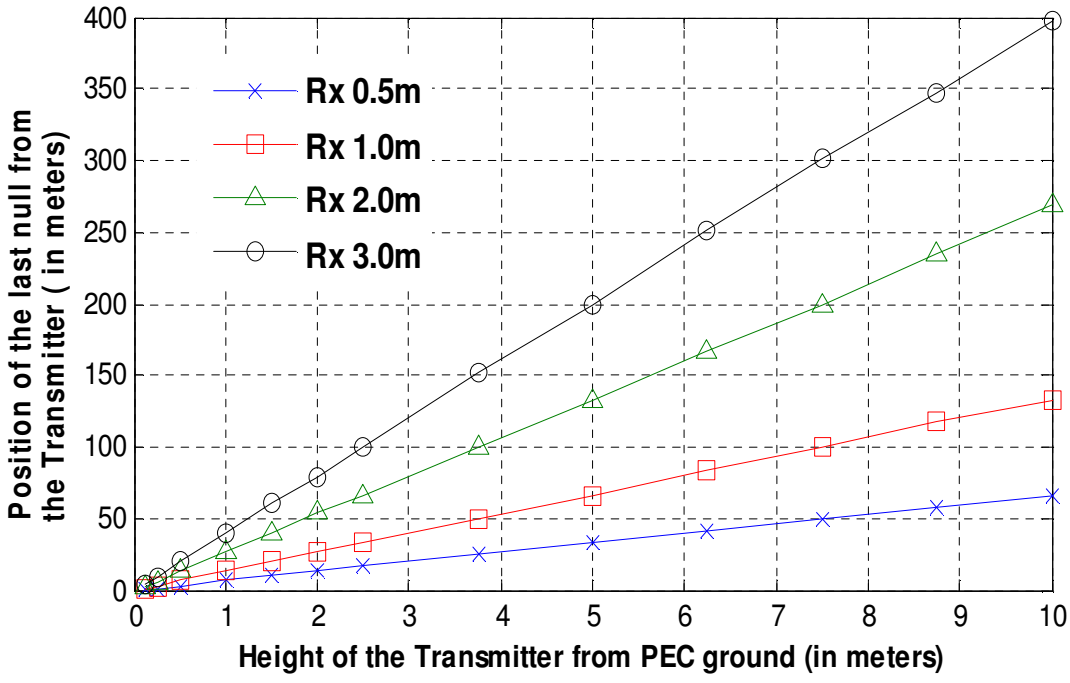

Figure 11: Variation of the Distance at which the last null of the theta-component

of the Electric field occurs, with respect to the height of the vertically oriented transmitting antenna above the PEC ground plane.

For sufficiently large D, we can approximate the above Eq. 17 using the small argument approximation for $\tan(x) \approx x$, for $x \ll 1$, as,

$$\frac{2\pi H_{Tx}H_{Rx}}{\lambda D}\tan\frac{2\pi H_{Tx}H_{Rx}}{\lambda D} \approx \left(\frac{2\pi H_{Tx}H_{Rx}}{\lambda D}\right)^2 = 1$$
$$\Rightarrow D = \frac{2\pi H_{Tx}H_{Rx}}{\lambda} \tag{18}$$

The above Eq. 18, which determines the position of the last maxima, can be used as the criteria for the transition of the near-field to the far-field behavior of the above system. Figure 12 below, summarizes the position of the last maxima for different heights of the vertically oriented half-wave transmitting antenna above the PEC ground plane based on the simulation result using a full-wave electromagnetic simulator. The blue line with crosses, the red line with squares, the green line with triangles, and the black line with circles correspond to the position of the maxima (or in other words the transition region of the near-field and the far-field field) for the observation heights at 0.5m,1.0m, 2.0m, and 3.0m respectively. It can be seen that the position of the last maxima changes linearly with the height of the transmitting antenna above the ground plane and the lines in Fig. 12 below, agrees well as predicted by Eq. 18.

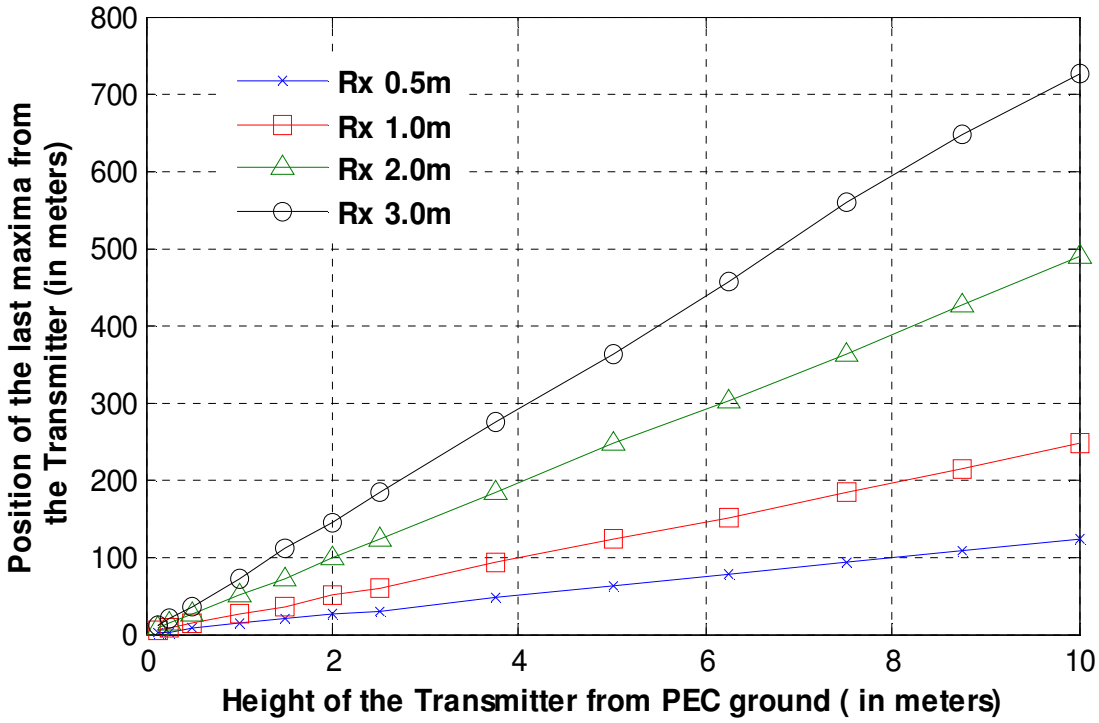

Figure 12: Variation of the Distance at which the last maxima of the theta-component of the Electric field occurs, with respect to the height of the vertically oriented transmitting antenna above the PEC ground plane.

The radial field component of the electric field as can be seen from Fig. 9 above is given by,

$$E_r = E_{r_1} + E_{r_2}$$
$$= \left(E_{z_1}(\theta_1)\cos\theta + E_{x_1}(\theta_1)\sin\theta\right) + \left(E_{z_2}(\theta_2)\cos\theta + E_{x_2}(\theta_2)\sin\theta\right) \quad (19)$$

For distance r » λ/2π, i.e., for distance further than the very reactive near-field of the antenna, the contribution due to where the contribution due to 1/r and $1/r^2$ terms are negligible. Using the approximation of r_1 as given in Eq. 9, and neglecting the 1/r and $1/r^2$ terms, E_{r1} can be approximated as,

$$
\begin{aligned}
E_{r_1} = \eta Idl\ \frac{e^{-j\beta r_1}}{4\pi r_1}\Bigg[& -\sin^2\theta_1 \cos\theta \left(j\beta + \frac{1}{r_1} + \frac{1}{j\beta r_1^2} \right) \\
& + \cos^2\theta_1 \cos\theta \left(\frac{2}{r_1} + \frac{2}{j\beta r_1^2} \right) \\
& + \sin\theta_1 \cos\theta_1 \sin\theta \left(j\beta + \frac{3}{r_1} + \frac{3}{j\beta r_1^2} \right) \Bigg]
\end{aligned} \tag{20}
$$

$$
\approx\ j\beta\eta Idl \frac{e^{\frac{-j2\pi D}{\lambda}}}{4\pi D} e^{\frac{-j2\pi}{\lambda}\frac{\left(H_{Tx}^2 + H_{Rx}^2\right)}{2D}} e^{\frac{j2\pi}{\lambda}\frac{H_{Tx}H_{Rx}}{D}}\ \sin\theta_1 \left[-\sin\theta_1 \cos\theta + \cos\theta_1 \sin\theta \right]
$$

For distances sufficiently large $\theta \rightarrow \pi/2$, $\theta_1 \rightarrow \pi/2$, $\theta_2 \rightarrow \pi/2$ and hence $\sin\theta$, $\sin\theta_1$ and $\sin\theta_2$ can be approximated to be equal to 1. On the other hand for $H_{Tx} > H_{Rx}$, the following approximations can be made regarding the cosine of the angles,

$$
\begin{aligned}
\cos\theta &\approx \frac{H_{RX}}{D} \\
\cos\theta_1 &\approx -\frac{H_{TX} - H_{RX}}{D} \\
\cos\theta_2 &\approx \frac{H_{TX} + H_{RX}}{D}
\end{aligned} \tag{21}
$$

Thus E_r can be modified as,

$$E_r = E_{r_1} + E_{r_2}$$

$$\approx j\beta\eta Idl \frac{e^{\frac{-j2\pi D}{\lambda}}}{4\pi D} e^{\frac{-j2\pi}{\lambda}\frac{\left(H_{Tx}^2 + H_{Rx}^2\right)}{2D}} \left[\begin{array}{l} e^{\frac{j2\pi H_{Tx}H_{Rx}}{\lambda D}} \left(-\frac{H_{RX}}{D} - \frac{H_{TX} - H_{RX}}{D} \right) \\ + e^{-\frac{j2\pi H_{Tx}H_{Rx}}{\lambda D}} \left(-\frac{H_{RX}}{D} + \frac{H_{TX} + H_{RX}}{D} \right) \end{array} \right] \quad (22)$$

$$= \beta\eta Idl H_{TX} \frac{e^{\frac{-j2\pi D}{\lambda}}}{2\pi D^2} e^{\frac{-j2\pi}{\lambda}\frac{\left(H_{Tx}^2 + H_{Rx}^2\right)}{2D}} \sin\frac{2\pi H_{Tx}H_{Rx}}{\lambda D}$$

As can be seen from Fig. 4 above that there is sine oscillation instead of cosine as in the case of the theta component of the field. The position where the null in the magnitude of the radial component of the Electric field appears is given by,

$$\sin\frac{2\pi H_{Tx}H_{Rx}}{\lambda D} = 0$$

$$\Rightarrow \frac{2\pi H_{Tx}H_{Rx}}{\lambda D} = m\pi \ , m \in \mathbf{I} \quad (23)$$

$$\Rightarrow D = \frac{2H_{Tx}H_{Rx}}{m\lambda}$$

The position of the last null for the radial component of the Electric field appears at,

$$D = \frac{2H_{Tx}H_{Rx}}{\lambda} \ , \quad (24)$$

This distance is half the distance compared to the distance for the theta component of the electric field which is given by Eq. 15. For distances D from the Transmitting antenna sufficiently far away, so that the observation point is in the far-field of the transmitting

antenna, the field decays monotonically without any oscillations. We can approximate the far field using the approximation based on sin X ≈ X as,

$$E_r \approx \beta\eta Idl \frac{H_{Tx}^2 H_{Rx}}{\lambda D^3} e^{\frac{-j2\pi D}{\lambda}} e^{\frac{-j2\pi\left(H_{Tx}^2+H_{Rx}^2\right)}{2D}} \tag{25}$$

Thus in the far-field the radial component of the electric field decays as $1/r^3$. Another interesting point to note is that the radial component of the field increases by square of the height of the receiver above the ground. Thus lower the H_{Tx}, lower is the radial component of the field compared to the theta component. This is demonstrated in Fig. 3 above. The ratio of the radial component to the theta component of the field is given as,

$$\left|\frac{E_r}{E_\theta}\right| = 2\pi \frac{H_{Tx}^2 H_{Rx}}{\lambda D^2} \tag{26}$$

The distances from the transmitter where the radial component of the Electric field is 40dB below the theta component of the field is shown in Fig.13 below. It can be seen that it changes linearly with the height of the Transmitter above ground plane. This is also predicted by Eq. 27 below. The explicit distance is given by,

$$\begin{aligned} & 2\pi \frac{H_{Tx}^2 H_{Rx}}{\lambda D^2} = \frac{1}{100} \\ & \Rightarrow D = 10 H_{Tx} \sqrt{\frac{2\pi H_{Rx}}{\lambda}} \end{aligned} \tag{27}$$

At the operating frequency of 1.0 GHz, the above Eq. 27 simplifies to,

$$D = 45.765\, H_{Tx} \sqrt{H_{Rx}} \tag{28}$$

The results predicted by Eq. 27 agree well with the simulated results in Fig. 13 below. The blue line with crosses, the red line with squares, the green line with triangles, and the black line with circles in Fig. 13 below correspond to the position where the radial component of the field is 40dB below the theta component of the electric field for the observation heights at 0.5m, 1.0m, 2.0m, and 3.0m respectively. However it should be kept in mind that Eq. 27 is valid when the near-field variation with peaks and nulls are absent, i.e. the observation point is in the far-field where the roll-off for the theta component of the field is 1/r and the radial component of the field is $1/r^3$ .In other words there is an additional constraint that D has to satisfy i.e. D has to be greater than Eq. 15. Thus Eq. 28 provides a further upper bound on the near-field region which might be necessary for some applications where the radial component of the field is not desirable at all.

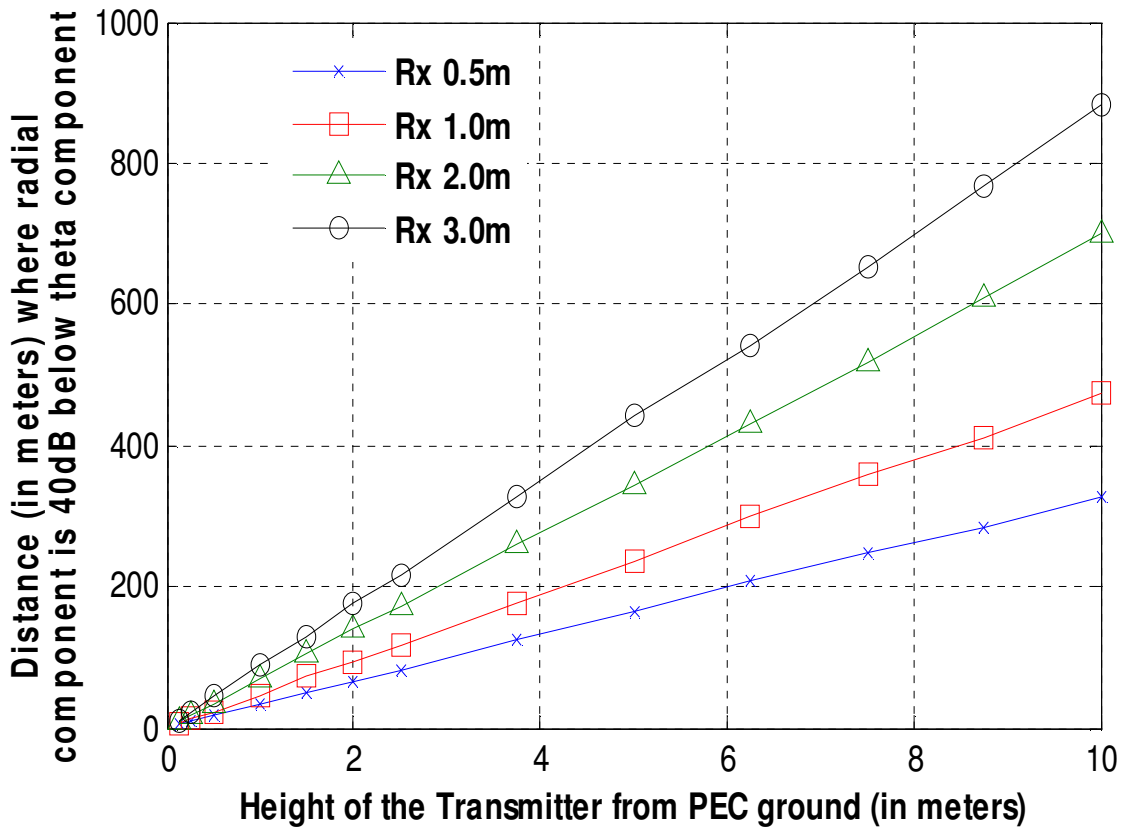

Figure 13: Variation of the Distance at which the radial component is 40dB below the theta component of the Electric field, with respect to the height of the vertically oriented transmitting antenna above the PEC ground plane.

If we choose the criterion based on the fact that the radial component is assumed to be below the theta component by 60dB Eq. 26 boils down to,

$$D = 144.72\, H_{Tx} \sqrt{H_{Rx}} \tag{29}$$

This is shown in Fig.14 below and the result predicted by the Eq. 29 agrees well with Fig. 14 below. The blue line with crosses, the red line with squares, the green line with triangles, and the black line with circles in Fig. 14 below correspond to the position

where the radial component of the field is 60dB below the theta component of the electric field for the observation heights at 0.5m, 1.0m, 2.0m, and 3.0m respectively. We observe that the far-field changes linearly with the height of the Transmitter above the PEC ground plane.

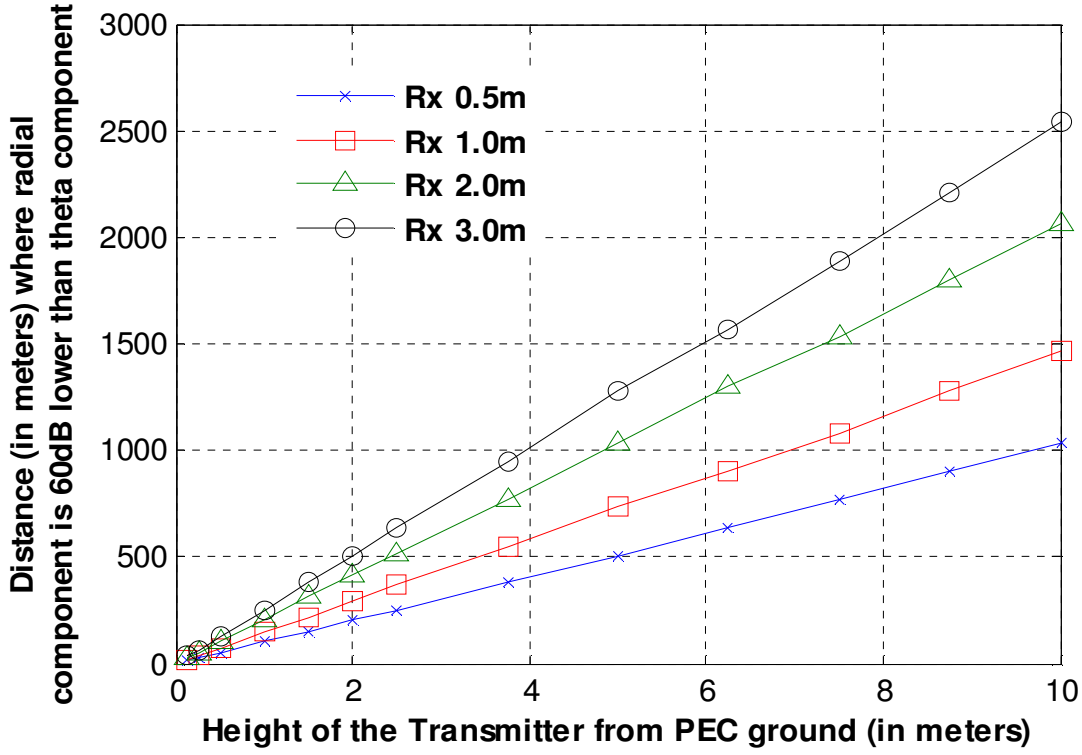

Figure 14: Variation of the Distance at which the radial component is 60dB below the theta component of the Electric field, with respect to the height of the vertically oriented transmitting antenna above the PEC ground plane.

Another interesting thing that is to be observed is that the position of this far-field is not linear with respect to the height of the observation point above the ground; instead it has a parabolic variation.

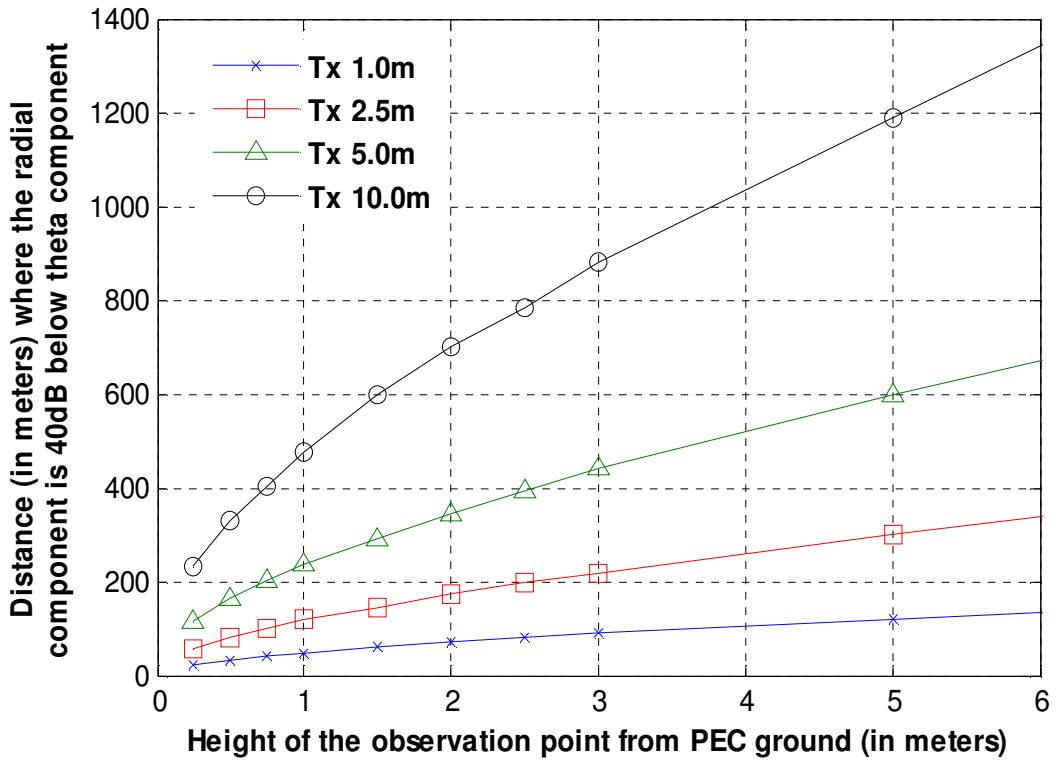

Figure 15: Variation of the Distance at which the radial component is 40dB below the theta component of the Electric field, with respect to the height of the receiver (field observation position) above the PEC ground plane.

This is predicted by Eq. 27-29. Fig.15 below shows the position at which the radial component of the electric field is 40dB below the theta component with respect to the height of the receiver from the PEC ground plane. The blue line with crosses, the red line with squares, the green line with triangles, and the black line with circles in fig. 13 below correspond to the position where the radial component of the field is 40dB below the theta component of the electric field for the heights of the vertically oriented transmitter

height at 1.0m, 2.5m, 5.0m, and 10.0m respectively. Similarly Fig. 16 shows the distance from the transmitter at which the radial component of the electric field is 60 dB below the theta component of the electric field with respect to the height of the receiver from the PEC ground plane. Note that they both exhibit the parabolic variation.

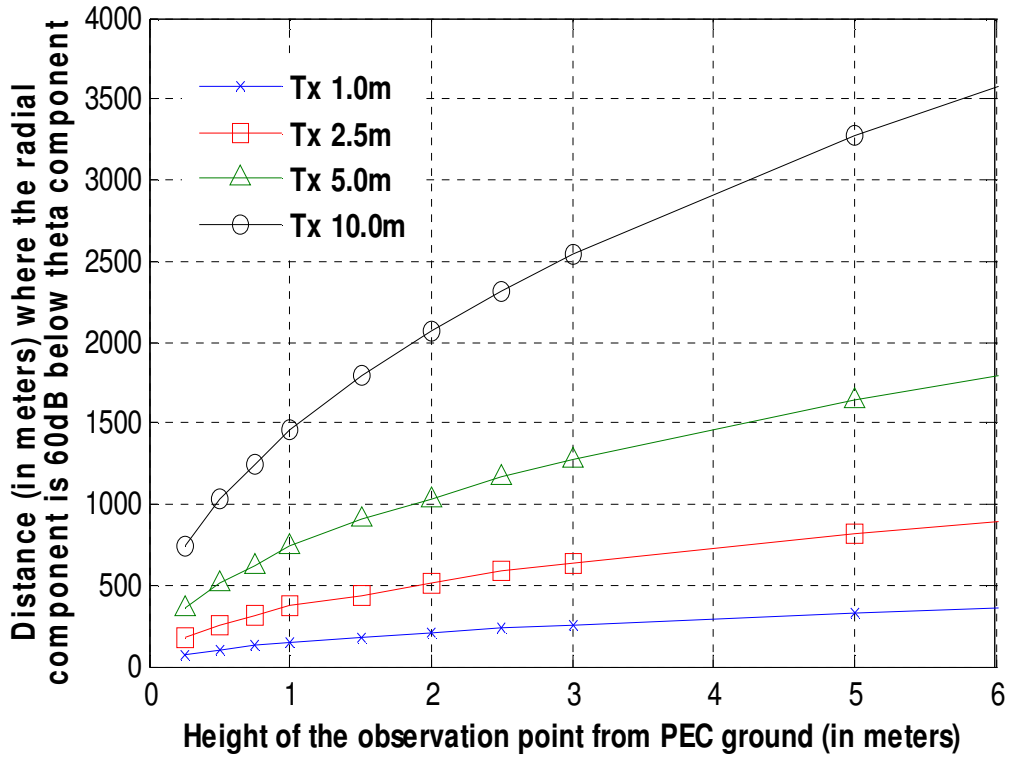

Figure 16: Variation of the Distance at which the radial component is 60dB below the theta component of the Electric field, with respect to the height of the receiver (field observation position) above the PEC ground plane.

2.3 Horizontal Dipole above PEC ground

2.3.1 Analysis of radiated field components

Now we consider a horizontally oriented half-wave center fed dipole antenna at a frequency of 1GHz, oriented horizontally over a PEC ground plane. The simulation setup is same as in Fig.1 shown above. In this case the direction of the image source is oriented in the opposite direction with respect to the original radiating dipole antenna. The Phi component of the electric field due to a Hertzian dipole oriented horizontally above PEC ground plane is given below as,

$$E_{\phi} = -\eta I dl \left[\frac{e^{-j\beta r_1}}{4\pi r_1} \left(j\beta + \frac{1}{r_1} + \frac{1}{j\beta r_1^{\,2}} \right) - \frac{e^{-j\beta r_2}}{4\pi r_2} \left(j\beta + \frac{1}{r_2} + \frac{1}{j\beta r_2^{\,2}} \right) \right] \tag{30}$$

where η is the impedance of the free-space, β is the wave number , I X dl is the dipole moment. The distances r_1 and r_2 as given in Eq.9 & 10 correspond to the distance of the observation point from the dipole and its image respectively. For sufficiently large values of r_1 and r_2 compared to the height of the transmitter and the observation point, the above Eq. 30 can be approximated using Eq. 11 & 12 as follows,

$$E_\phi \approx -j\beta\eta Idl\left[\frac{e^{-j\beta r_1}}{4\pi r_1}-\frac{e^{-j\beta r_2}}{4\pi r_2}\right]$$

$$=-\frac{j\beta\eta Idl}{4\pi D}e^{\frac{-j2\pi D}{\lambda}}e^{\frac{-j2\pi}{\lambda}\frac{\left(H_{Tx}^2+H_{Rx}^2\right)}{2D}}\left[e^{\frac{j2\pi}{\lambda}\frac{H_{Tx}H_{Rx}}{D}}-e^{\frac{-j2\pi}{\lambda}\frac{H_{Tx}H_{Rx}}{D}}\right] \tag{31}$$

$$=\frac{\beta\eta Idl}{2\pi D}e^{\frac{-j2\pi D}{\lambda}}e^{\frac{-j2\pi}{\lambda}\frac{\left(H_{Tx}^2+H_{Rx}^2\right)}{2D}}\sin\frac{2\pi H_{Tx}H_{Rx}}{\lambda D}$$

We observe that the magnitude of the Phi component of the Electric field exhibits a sinusoidal oscillation just like in the case of the vertical dipole with deep nulls and peaks. The blue solid line in Fig. 17 gives the simulated result of the variation of the magnitude of the Φ-component of the Electric field with the distance of the observation point from the transmitter when the transmitting half-wave dipole is placed 5m above the PEC ground plane and the Receiving observation point of the field is at 2m from the PEC ground plane. The position of the nulls using Eq. 31, are given by,

$$\sin\frac{2\pi H_{Tx}H_{Rx}}{\lambda D}=0$$

$$\Rightarrow \frac{2\pi H_{Tx}H_{Rx}}{\lambda D}=m\pi \ , m\in \mathbf{I} \tag{32}$$

$$\Rightarrow D=\frac{2H_{Tx}H_{Rx}}{m\lambda}$$

The position of the last null, after which the field decays monotonically without any further oscillations, corresponds to m=1, is given by,

$$D=\frac{2H_{Tx}H_{Rx}}{\lambda} \tag{33}$$

We see that the last null corresponding to the horizontal dipole in the blue solid line in Fig. 17 is at a distance of 66.67m from the transmitting dipole and it satisfies the value predicted by the eq. 33. After 66.67m the field decays constantly without any further oscillations with peaks and nulls. Compared with the vertical dipole case as given in Eq. 15, the position of the last null for the horizontal dipole above PEC ground is in fact half the distance but it also varies linearly with the height of the transmitting antenna above the ground. The red dotted line in Fig. 17 shows the variation of the θ-component of the Electric field with distance for a vertically oriented dipole placed at the same height of 5m above the PEC ground plane. We see the last null in this case is at 133.33m from the Transmitting antenna. We notice two further differences in the field variation for the case of the horizontally oriented dipole (blue solid line) and the vertically oriented dipole (red dotted line). In the very near-field of the antenna, the magnitude of the Φ-component of the Electric field due to the horizontally placed half-wave dipole antenna is much higher than the θ-component of the Electric field due to the vertically placed half-wave dipole antenna placed at the same height above the PEC ground plane. At a distance of 0.1m from the transmitting antenna, the field due to horizontally placed antenna is almost 35dB stronger than the field due to vertically oriented antenna. This difference decreases but continues around 10m after which the magnitude of the field strengths is almost the same. The second difference between the two orientations is in the far-field of the antenna. For the vertically oriented antenna the far-field decays as 1/D where D is the horizontal distance between the transmitter and the receiving observation point. But for the horizontally oriented antenna the field decays as $1/D^2$, as can be seen in the blue solid line in Fig. 17 below. Using the approximation of sin X ≈ X, the far-field of the Φ-

component of the electric field for the horizontally oriented dipole above the PEC ground can be derived from Eq. 31 as,

$$E_{\phi} \approx \beta\eta Idl \frac{H_{Tx}H_{Rx}}{\lambda D^2} e^{\frac{-j2\pi D}{\lambda}} e^{\frac{-j2\pi\left(H_{Tx}^2+H_{Rx}^2\right)}{2D}} \tag{34}$$

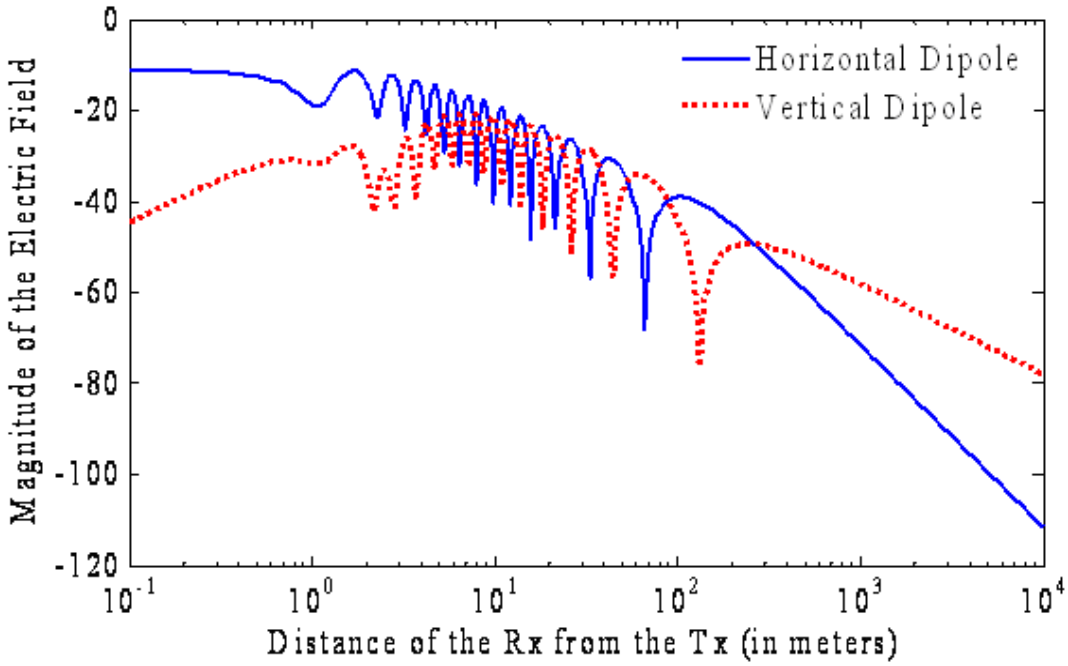

Figure 17: Phi component of the Electric field due to a horizontally oriented half-wave dipole antenna located 5m above the PEC ground plane. The field observation is at 2m from the PEC ground.

The radial field however, unlike the case of the vertically oriented antenna is extremely lower (almost 150dB down) compared to the Φ-component of the Electric field for the horizontally oriented dipole antenna. So for the horizontally oriented dipole antenna we do not analyze the radial component of the field and the different far-field criterion that has been used for the vertically oriented dipole antenna before.

2.3.2 Phenomenon of Height-Gain associated with the radiated field

It can be seen from Eq. 34 that the magnitude of the far-field for the horizontally oriented dipole antenna above PEC ground plane increases linearly with the height of the transmitting antenna above the PEC ground. The blue broken line, red dotted line, and the green solid line in Fig. 18 below shows the Φ component of the electric field for the Transmitting dipole antenna at a height of 0.25m, 2.0m, and 10.0m respectively. The increment of the magnitude in the far-field is around 6dB per octave. It can be seen from Fig. 18 below when the transmitter is changed from 0.25m above PEC to 2.0m above PEC, i.e. the far-field magnitude at a distance of 1Km from the Transmitter changes from -96dB to -80dB.

The gain in the field due to the height of the antenna above PEC ground can be attributed to the fact that as the transmitting antenna is brought higher up above the ground the main beam of the far-field radiation pattern shifts towards the ground, along with more lobes i.e. more peaks and nulls. Thus when the antenna is placed 0.25m above ground the beam of the far-field radiation pattern that is closest to the ground plane is tilted at an elevation angle of 17 degrees from the ground plane. When the antenna is brought up to 2.0m, the beam closest to the ground is tilted at an angle of 2 degrees.

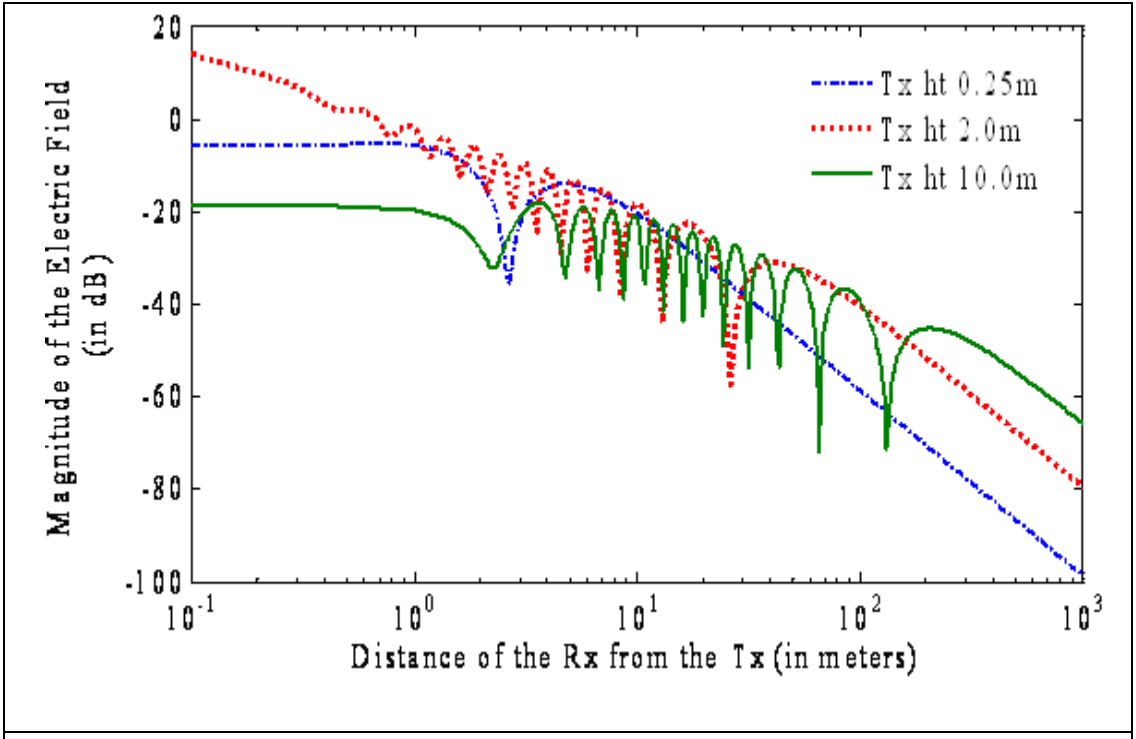

Figure 18: Phi component due to a horizontally oriented half-wave transmitting dipole antenna above a PEC ground plane for different heights of the transmitting antenna. The field observation point is located at 2m from the PEC ground.

When the antenna is brought further up to 10m, the beam nearest to the ground is tilted at an elevation angle of 0.45 degrees. Based on the above phenomenon it is easy to conclude that one should position a horizontally oriented antenna used for wireless communication as high as possible, without taking the distance at which the far-field starts into consideration. As we have seen for both the vertically and horizontally oriented antenna, the higher the position of the transmitting antenna above the ground plane the further is the distance at which the far-field starts after which the field decays with a constant slope. In the near-field as has been stated before, the field oscillates wildly with large peaks and nulls. In most of the study related to wireless communication we are

considered with the far-field but not much attention is paid to the relation between the height of the antenna above the ground plane and the position of the transition of the near-field to far-field. The objective of this thesis is to incorporate these ideas so that one can take a judicious decision in the optimum position of the transmitting antenna above the ground plane. This is more clarified by an example. Let's say a transmitting antenna operating at 1GHz is placed 20m above the ground plane which his typically the case, while the receiver is at 2m above the ground plane. Using Eq.33 the position of the last null will be at a distance of 266.67m from the transmitter. As will be shown later in Eq. 37, the far-field starts after around 602.67m. The typical coverage of a cellular communication is around 1~3 Km. Thus almost half of the cell size is in the near-field of the antenna where the field varies wildly with peaks and nulls. Many literatures call them as large scale fading. Beam-forming or other array processing techniques that has been widely used in wireless communication is thus difficult to be implemented successfully in this region as, it those techniques assume that the receiver is in the far-field of the transmitter. Thus it would be more judicious to bring the transmitting antenna closer to the ground to around 5m than placing it at 20m above the ground, though in the far-field the magnitude of the field is smaller in this case than the former one. In this case however the far-field starts around 150.67m which might be acceptable to some system designers.

2.3.3 Wave impedance of the radiated field

Fig.19 below shows the impedance of the wave for different height of the horizontally oriented transmitting antenna above the PEC ground plane. It can be seen that as the transmitting antennas is placed higher above the ground plane the real part of the impedance converges to η_o at much further distance.

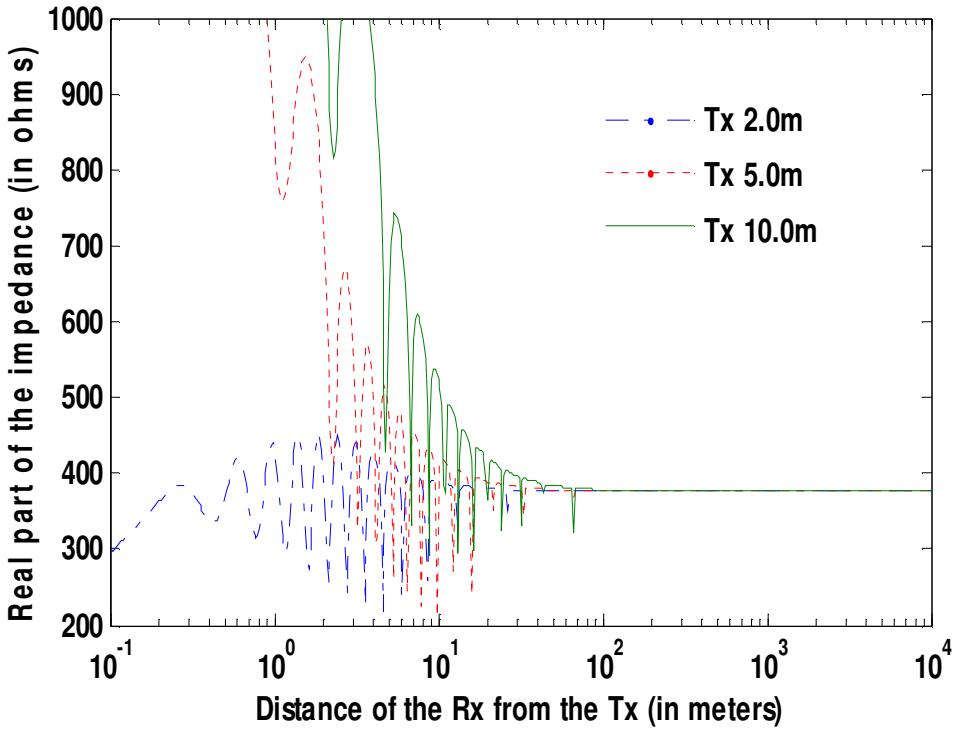

Figure 19: Variation of the real part of the wave impedance with the distance from the transmitter for a half-wave dipole antenna horizontally oriented above PEC ground plane.

Thus when the transmitter is at a height of 2m as shown in blue broken line, the real part of impedance converges at around 10m from the transmitting antenna. When the transmitting antenna is placed higher up to 5m above PEC ground as shown in red dotted line, the distance at which the real part of the impedance converges is approximately at around 25m. When the transmitting antenna is placed further above at 10m as shown in green solid, the real part of the impedance converges at around 50m from the transmitter.

It can be seen from the above results, that for the above configuration, after approximately five times the height of the transmitter from the PEC ground plane, the real part of the impedance converges to η_o. The region lesser than this distance can be referred to as the very near-field of the antenna system. Thus the very near-field of the antenna system also changes linearly with the height of the antenna above the ground plane and not as square of it. The impedance and the Poynting vector is a complex quantity with significant imaginary portion in this region. Beyond this region however the impedance is close to η_o and the phase of the impedance is almost zero. However the magnitude of the field still exhibits peaks and nulls and does not decay as 1/D as it should be in the far-field. This is clearly shown in Fig, 20 below where the horizontally oriented half-wave transmitting dipole antenna is placed at a height of 5m above the PEC ground plane and the observation point is 2m above ground plane. The blue solid line indicates the magnitude of the Phi component of the Electric field. It can be seen that the far-field behavior occurs at a distance of around 150.67m from the transmitter. The green broken line indicates the real part of the impedance which converges to η_o at around 25m.

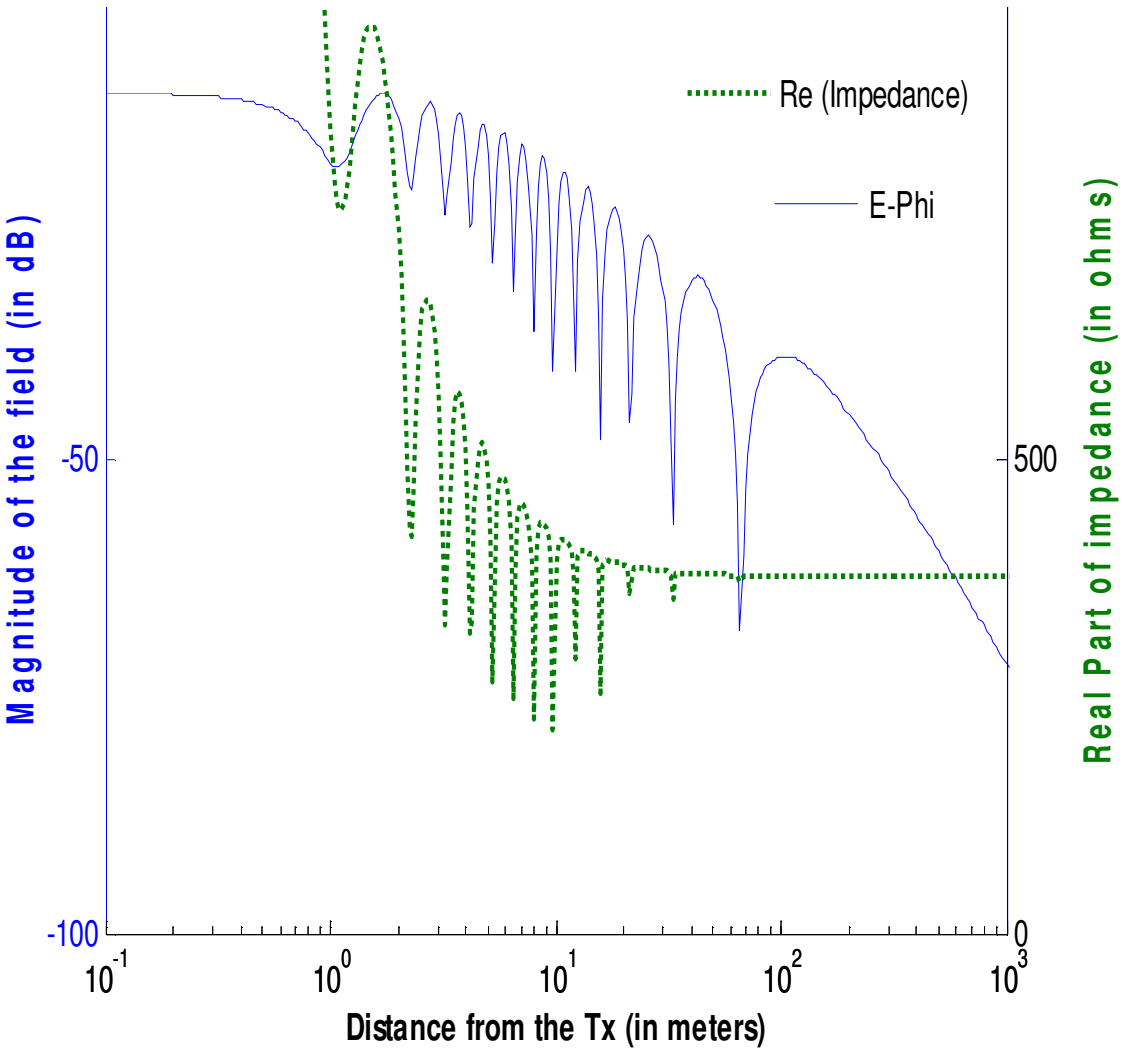

Figure 20: Comparison of the very near field and the near field for the horizontally oriented half-wave antenna above the PEC ground plane as determined by the convergence of the real part of the impedance and the constant roll-off of the magnitude of the electric field as $1/D^2$ respectively.

2.3.4 Field components when the height of the receiver is varied.

As in the vertically oriented dipole case, it is of some interest to observe the variation of the field with the change in the height of the observation point, keeping the height of the transmitting antenna at the same location. The transmitting antenna is placed 5m above the PEC ground plane.

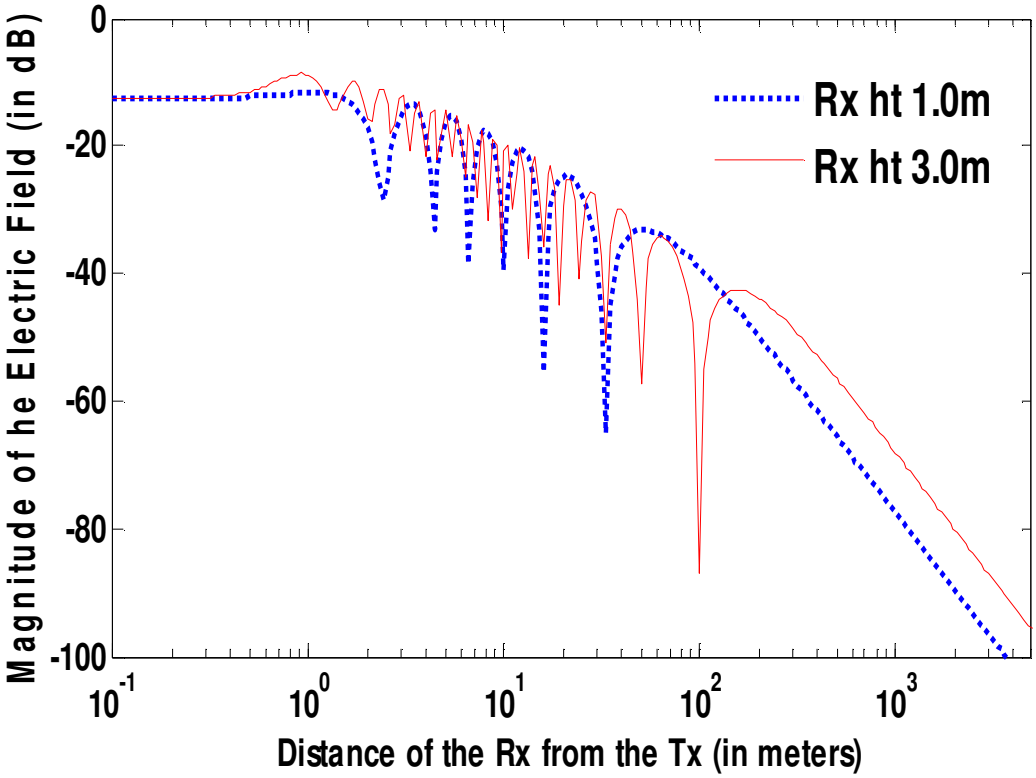

Figure 21: Comparison of the magnitude of the Phi component of the Electric field for various observation heights and for fixed transmitter height above the PEC ground plane.

The blue dotted line in Fig.21 shows the magnitude of the Φ component of the Electric field when the observation height is at 1.0m. For this case the far-field starts approximately from 75m. As the receiver height is moved higher up to 3m, as shown by the red solid line in Fig. 21 below, the far-field shifts 3 times further away and starts from 225m.

Figure 22 below, summarizes the position of the last null for different heights of the horizontally oriented half-wave transmitting antenna above the PEC ground plane based on the simulation result using a full-wave electromagnetic simulator.

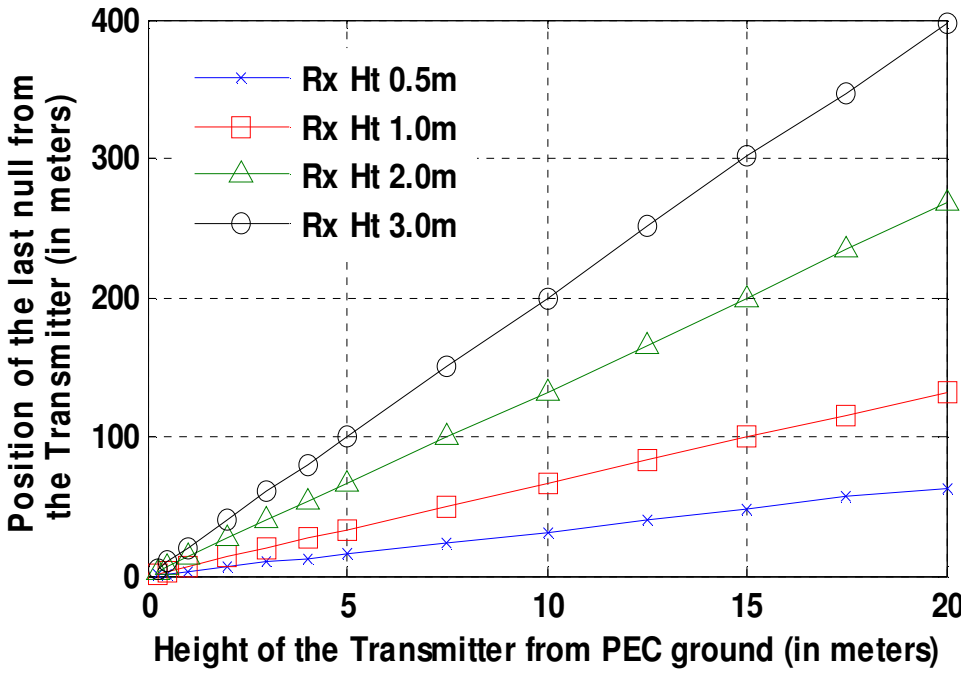

Figure 22: Variation of the Distance at which the last null of the theta-component

of the Electric field occurs, with respect to the height of the horizontally oriented transmitting antenna above the PEC ground plane.

The blue line with crosses indicates the position of the last null for the field observation height at 0.5m above the ground plane. The red line with squares, the green line with triangles and the black line with circles correspond to the field observation heights of 1.0m, 2.0m, and 3.0m respectively. It can be seen that the position of the last null changes linearly with the height of the transmitting antenna above the ground plane and all the lines in Fig. 22 below, agrees with the predicted formulae given by Eq. 33.

It can be seen from Fig.17, 18 that after the last null, the magnitude of the electric field reaches maxima after which the field rolls off at $1/D^2$. This behavior is very similar to the vertically oriented dipole antenna as described above, but the positions of the maxima are different from the vertically oriented case. The position of this determined by the value of D which satisfies the following,

$$\frac{\partial}{\partial D}\left(\frac{\sin\frac{2\pi H_{Tx}H_{Rx}}{\lambda D}}{D}\right)=0$$

$$\Rightarrow \frac{-\frac{2\pi H_{Tx}H_{Rx}}{\lambda D}\cos\frac{2\pi H_{Tx}H_{Rx}}{\lambda D}-\sin\frac{2\pi H_{Tx}H_{Rx}}{\lambda D}}{D^2}=0 \qquad (35)$$

$$\Rightarrow \tan\frac{2\pi H_{Tx}H_{Rx}}{\lambda D}=-\frac{2\pi H_{Tx}H_{Rx}}{\lambda D}$$

The solution to the above Equation is given by,

$$\frac{2\pi H_{Tx} H_{Rx}}{\lambda D} = 2.03 \tag{36}$$

$$\Rightarrow D = 3.1 \frac{H_{Tx} H_{Rx}}{\lambda}$$

The above Eq. 36, which determines the position of the last maxima, can be used as the criteria for the transition of the near-field to the far-field behavior of the above system. Figure 23 below, summarizes the position of the last maxima for different heights of the horizontally oriented half-wave transmitting antenna above the PEC ground plane based on the simulation result using a full-wave electromagnetic simulator.

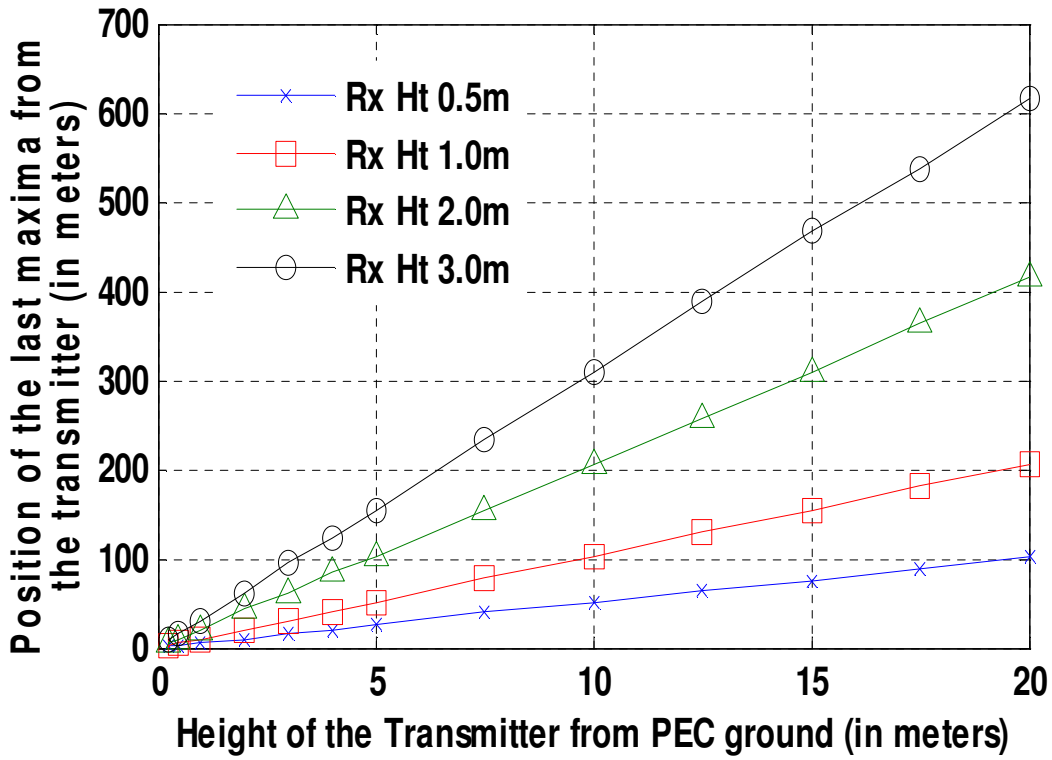

Figure 23: Variation of the Distance at which the last maxima of the theta-component

of the Electric field occurs, with respect to the height of the vertically oriented transmitting antenna above the PEC ground plane.

The blue line with crosses, the red line with squares, the green line with triangles, and the black line with circles correspond to the position of the maxima (or in other words the transition region of the near-field and the far-field field) for the observation heights at 0.5m,1.0m, 2.0m, and 3.0m respectively. It can be seen that the position of the last maxima changes linearly with the height of the transmitting antenna above the ground plane and the lines in Fig. 23 below, agrees exactly with the predicted formulae given by Eq. 36.

Yet another different criterion based on the similar phenomenon can be derived to characterize the transition of the near-field to the far-field. It is to be noted that after the last null, the magnitude of the Φ-component of the electric field reaches a maximum after which it rolls-off as $1/r^2$, which is the desired far-field behavior. The new criterion is based on the distance, at which the Φ-component of the electric field is within -3dB of the $1/D^2$ decay and is given by the condition,

$$20\log\left(\frac{\sin\frac{2\pi H_{Tx}H_{Rx}}{\lambda D}}{\frac{2\pi H_{Tx}H_{Rx}}{\lambda D}}\right) = -3 \qquad (37)$$

$$\Rightarrow \frac{2\pi H_{Tx}H_{Rx}}{\lambda D} = 1.39$$

$$\Rightarrow D = 4.52\frac{H_{Tx}H_{Rx}}{\lambda}$$

It should be noted that the criterion given by, Eq. 36 is a strict lower bound on the position of the transition of the near-field to far-field.

3. ANTENNAS ABOVE IMPERFECTLY CONDUCTING GROUND

3.1 Introduction

We now consider the field radiated by both vertically and horizontally radiating dipole antenna over an imperfectly conducting ground. Many researchers have derived several expressions valid for different regions of the radiating Hertzian dipole above a conducting half-space which have been nicely summarized in Banos [1966], Brekhovskikh [1960], Collin and Zucker [1969], Tyras [1960]. For the sake of continuity and the discussion, in this section we derive some closed form approximate yet simple formulas for the behavior of the Electric field in the far-zone of the antenna and the position where the transition between the near-field and the far-field occurs. Cylindrical coordinate system has been used for the calculation of the field and is shown in Fig. 24. The Hertzian dipole antenna (A) is situated in medium-1 at a height z_a above the ground. Medium-1(which is normally air) has the propagation constant k_1 is the upper half-space and Medium-2 with propagation constant k_2 covers the lower half-space. The complex propagation constant k of a medium with permittivity ε and conductivity σ is given by,

$$k^2 = \frac{1}{c^2}\left(\varepsilon\,\omega^2 + j\omega\sigma\right) \tag{38}$$

The field observation point (B) is at a height z from the air-ground interface and at a

radial distance of ρ from the transmitting antenna. The distances of the observation point B, from the source point A and the image of the source A´, given as R_1 and R_2 respectively by,

$$R_1^2 = \rho_0^2 + (z_a - z_b)^2 \tag{39}$$

$$R_2^2 = \rho_0^2 + (z_a + z_b)^2 \tag{40}$$

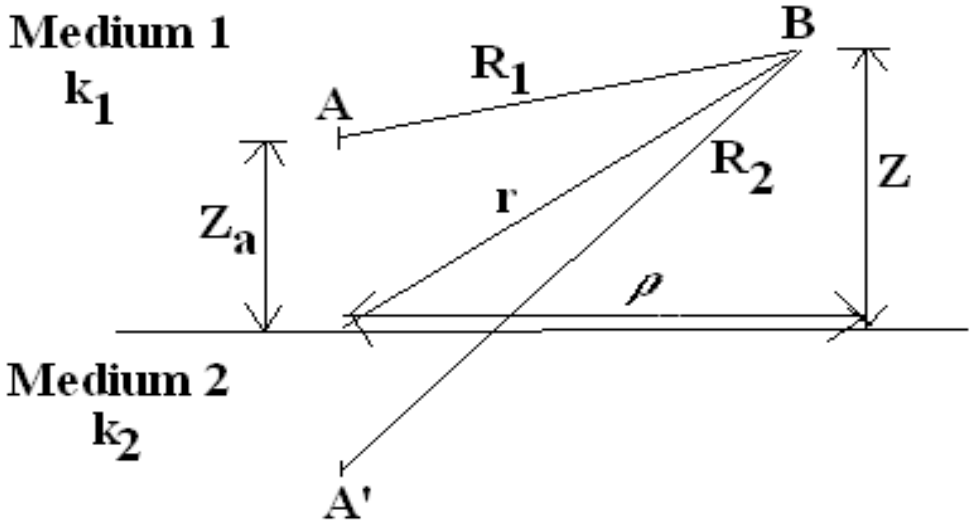

Figure 24: Coordinate system for the antenna over imperfectly conducting ground.

3.2 Vertical Dipole above imperfectly conducting ground

First we consider the vertically oriented Hertzian dipole antenna over the real ground. The Hertzian vector in the upper medium, denoted by Π_1 is along the z-direction. It can be decomposed into primary stimulation that becomes singular at the dipole and the secondary stimulation that is regular throughout due to the currents induced in the ground. Following Sommerfeld's derivation given in Sommerfeld [1909] and Sommerfeld [1926], of the solution of Hertzian potential for the vertically oriented Hertzian dipole above conducting earth one can write the Hertzian potentials as,

$$\Pi_1 = \Pi_{pr} + \Pi_{sec} \tag{41}$$

The primary component of the Hertzian potential is given as,

$$\Pi_{pr} = \frac{e^{jk_1 R_1}}{R_1} \tag{42}$$

while the secondary component is given as,

$$\Pi_{sec} = \int_{\lambda=0}^{\lambda=\infty} \lambda d\lambda \, J_o(\lambda\rho) \, \frac{k_2^2 l - k_1^2 m}{k_2^2 l + k_1^2 m} \, \frac{e^{-(z_a+z)l}}{l}$$

$$= \int_{\lambda=0}^{\lambda=\infty} \lambda d\lambda \, J_o(\lambda\rho) \left(1 - \frac{2k_1^2 m}{k_2^2 l + k_1^2 m} \right) \frac{e^{-(z_a+z)l}}{l} \tag{43}$$

where l and m is given by,

$$l = \sqrt{\lambda^2 - k_1^2} \tag{44}$$

$$m = \sqrt{\lambda^2 - k_2^2} \tag{45}$$

The derivation of Eqns. 41-43 by solving the half-space boundary value problem using Sommerfeld's Hertz vector potential is discussed in Appendix A and is also discussed in several literatures as in Miller et. al. [1972], Sarkar [1975].

In order to find the position where the far-field behavior of the antenna takes over the near-field rapid fluctuations, we need to make certain approximations of the secondary stimulation given by Eqn. 43. Last century saw great debates between several stalwarts regarding the various asymptotic approximations of the Electric field due to Hertzian dipole over a lossy half-space which have been nicely described by Collin [2004]. For the sake of continuity in the discussions and the validation of the simplified expressions used to calculate the position of the last null in the near-field as in the case of the antenna over perfectly conducting earth, we summarize in Appendix B, the derivation of the approximate formulas. Using the approximations stated in the appendix, the total Hertz vector potential along Z-direction, for a vertically oriented Hertzian dipole antenna over lossy earth is given as,

$$\Pi_1 = \frac{e^{jk_1R_1}}{R_1} - \frac{e^{jk_1R_2}}{R_2} + 2\frac{e^{jk_1R_2}}{{R_2}^2}\frac{jn^2}{k_1} \tag{46}$$

The Electric fields can now be calculated using the relation,

$$E = \nabla\nabla.\Pi_1 + {k_1}^2\Pi_1 \tag{47}$$

Thus the z-component of the Electric field is given as,

$$E_z(z) = \frac{\partial^2}{\partial z^2}\Pi_1 + k_1^2\Pi_1 \tag{48}$$

We note that,

$$\frac{\partial}{\partial z}\frac{e^{jk_1R_1}}{R_1} = \frac{z}{R_1}\frac{\partial}{\partial R_1}\left(\frac{e^{jk_1R_1}}{R_1}\right) = O\left(\frac{1}{R_1^2}\right) \tag{49}$$

Any further differentiation with respect to z will introduce higher order terms of $1/R_1$, which can be neglected for distances sufficiently far away from the antenna. Using the similar approximations as in the case of an antenna over a perfectly conducting ground, the z-component of the Electric field can be approximated as,

$$\begin{aligned} E_z &= k_1^2\left(\frac{e^{jk_1R_1}}{R_1} - \frac{e^{jk_1R_2}}{R_2}\right) \\ &\approx \frac{k_1^2}{\rho}e^{jk_1\rho}\left(e^{jk_1\frac{(z-z_a)^2}{2\rho}} - e^{jk_1\frac{(z+z_a)^2}{2\rho}}\right) \\ &= -2jk_1^2 e^{jk_1\frac{(z^2+z_a^2)}{2\rho}}\frac{e^{jk_1\rho}}{\rho}\sin\left(k_1\frac{z\,z_a}{\rho}\right) \end{aligned} \tag{50}$$

The radial component of the electric field is given by,

$$E_\rho = \frac{\partial^2}{\partial\rho\,\partial z}\Pi_1 \tag{51}$$

Now, we have,

$$\frac{\partial}{\partial z}\frac{e^{jk_1R_1}}{R_1} = \frac{z-z_a}{R_1}\frac{\partial}{\partial R_1}\left(\frac{e^{jk_1R_1}}{R_1}\right)$$

$$=(z-z_a)\left(jk_1\frac{e^{jk_1R_1}}{R_1^{\,2}}-\frac{e^{jk_1R_1}}{R_1^{\,3}}\right) \tag{52}$$

and,

$$\frac{\partial}{\partial\rho\partial z}\frac{e^{jk_1R_1}}{R_1} = (z-z_a)\frac{\rho}{R_1}\frac{\partial}{\partial R_1}\left(jk_1\frac{e^{jk_1R_1}}{R_1^{\,2}}-\frac{e^{jk_1R_1}}{R_1^{\,3}}\right)$$

$$=(z-z_a)\frac{\rho}{R_1}\left(-k_1^{\,2}\frac{e^{jk_1R_1}}{R_1^{2}}-3jk_1\frac{e^{jk_1R_1}}{R_1^{3}}+3\frac{e^{jk_1R_1}}{R_1^{4}}\right) \tag{53}$$

Similarly we have,

$$\frac{\partial}{\partial\rho\partial z}\frac{e^{jk_1R_2}}{R_2} = (z+z_a)\frac{\rho}{R_2}\left(-k_1^{\,2}\frac{e^{jk_1R_2}}{R_2^{\,2}}-3jk_1\frac{e^{jk_1R_2}}{R_2^{\,3}}+3\frac{e^{jk_1R_2}}{R_2^{\,4}}\right) \tag{54}$$

The third term in the Hertz potential in Eqn. 46 will introduce terms of $O(1/\rho^3)$. For distances sufficiently far away from the antenna we can neglect the higher order terms. When the transmitting antenna is located at a height greater than the field observation point as is usually the case for the cellular communication environment, the radial component of the electric field can be approximated as,

$$E_\rho=(z-z_a)\frac{\rho}{R_1}\left(-k_1^{\,2}\frac{e^{jk_1R_1}}{R_1^{\,2}}\right)-(z+z_a)\frac{\rho}{R_2}\left(-k_1^{\,2}\frac{e^{jk_1R_2}}{R_2^{\,2}}\right)$$

$$\approx\left(\frac{-k_1^{\,2}z}{\rho^2}\right)\left(e^{jk_1R_1}-e^{jk_1R_2}\right)+\left(\frac{k_1^{\,2}z_a}{\rho^2}\right)\left(e^{jk_1R_1}+e^{jk_1R_2}\right)$$

$$= 2k_1^2 e^{jk_1\frac{(z^2+z_a^2)}{2\rho}} \frac{e^{jk_1\rho}}{\rho^2}\left[z_a \cos\left(k_1 \frac{z z_a}{\rho} \right) + jz \sin\left(k_1 \frac{z z_a}{\rho} \right) \right]$$

$$\approx 2k_1^2 e^{jk_1\frac{(z^2+z_a^2)}{2\rho}} \frac{e^{jk_1\rho}}{\rho^2}\left[z_a \cos\left(k_1 \frac{z z_a}{\rho} \right) \right] \quad (55)$$

Eqns. 50 and 55 are the approximate results that we will be using in calculating the various criteria of the far-field and the near-to-far field transition. It is to be noted that the form of Eqn. 50 i.e. the E-z component of the electric field due to a vertically oriented Hertzian dipole over real ground is very similar to Eqn. 31 which is the field due to a horizontally oriented dipole over perfectly conducting ground. Thus in the radiating far-field the Ez component of the field due to a vertically oriented dipole decays as inverse of the square of the distance in contrast to the similar case above the PEC ground. Several arguments explaining this behavior is attributed to contribution of surface waves and the cancellation of the direct and the indirect rays. This had at times raised lots of controversy and debates. Henceforth this dissertation tries to avoid such a route and tries to go through some details along with the validation of simulations using commercial software package AWAS developed by Djordjevic et. al. [2002], which uses the Sommerfeld formulation.

The Figure below shows the components of the Electric field for a transmitting dipole antenna at a frequency of 1GHz. The antenna is placed 10m above the imperfectly conducting earth. The relative permittivity ε_r =4.0 and conductivity of σ = 2 X 10^{-4} mhos/m representing urban ground. Electric fields are calculated at a height of 2m from

the ground. The deep-blue line indicates the E-z component of the electric field calculated using AWAS. The light blue line indicates the E-z component of the electric field using Eqn. 50. We see for distances greater than approximately five times the height of the transmitter, the approximate eqn. matches with the simulation results. We observe that the magnitude of the electric field exhibits a sinusoidal oscillation with deep nulls and peaks. The predicted position of the last null D, after which the field decays monotonically without any further oscillations, is given by Eqn. 33 i.e.

$$D = \frac{2H_{Tx}H_{Rx}}{\lambda}.$$

We see that the position of the last null as indicated by the blue line in the figure below is at a distance of 133.33m from the transmitting dipole and it agrees with the predicted formulae. After 133.33m the field decays constantly as inverse of the distance square, without any further oscillations with peaks and nulls. This can also be seen from Eqn. 50 by substituting the approximation of sin X ≈ X, for sufficiently small X. It can also be seen that the magnitude of the far-field increases linearly with the height of the transmitting antenna above ground. The position of the last maxima after which the field decreases monotonically is given by Eqn. 36 i.e.

$$D = 3.1\frac{H_{Tx}H_{Rx}}{\lambda}.$$

Similarly Eqn. 37 i.e. $D = 4.52\frac{H_{Tx}H_{Rx}}{\lambda}$ can be used as the transition region between the near-field to the far-field based on the criteria where the far-field is within 3-dB of the $1/D^2$ roll-off. Thus we see that as in the case of the dipole above PEC ground, the position of the last null and the last maxima varies linearly with the height of the

transmitting antenna above the ground.

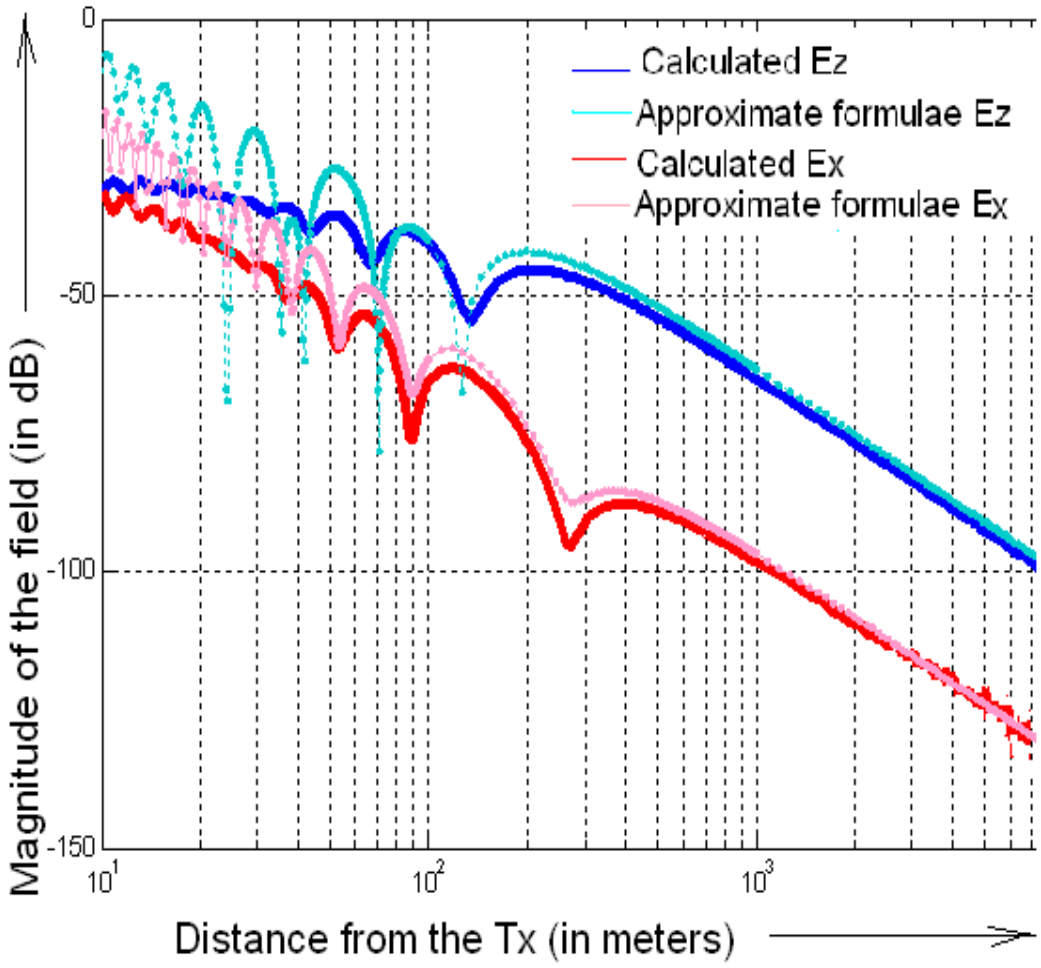

Figure 25: Comparison of the z-component and the radial component of the Electric field due to a vertically oriented Hertzian dipole using Eqns. 50 and 55 and a half-wave dipole when the transmitting antenna is placed 10m above urban soil and the field is observed 2m above the ground.

The red line indicates the E-x component of the electric field calculated using AWAS. The pink line indicates the E-x component of the electric field using Eqn. 55. The

magnitude of the E-x component of the Electric field exhibits a sinusoid oscillation with deep nulls and peaks. In the far-field the cosine term approaches unity and the field decays as inverse of the square of the distance as shown in the Fig. 25 above instead of $1/D^3$ decay as in the case of the vertical dipole above PEC ground. This is another major difference between the far-fields due to a vertically oriented dipole above imperfectly conducting ground and perfectly conducting ground. The predicted position of the last null D, is given by Eqn.15 i.e. $D = \frac{4H_{Tx}H_{Rx}}{\lambda}$ which is twice the distance compared to the case for the Z-component of the Electric field. The radial field also increases linearly with the height of the transmitter above the ground. For the above case of the transmitter and the receiver at a height of 10m and 2m from the ground respectively, the last null occurs at a distance of 266.67m from the transmitter. The position at which the far-field roll-off is within -3dB of the $1/D^2$ decay is also given as in Eqn. 16 as $D = \frac{8H_{Tx}H_{Rx}}{\lambda}$. Since the radial component of the electric field due to a vertically oriented dipole above the imperfect ground decays as $1/D^2$ rather than 1/D, the position of the last maxima is not the same as given in Eqn. 18. We thus have,

$$\frac{\partial}{\partial D}\left(\frac{\cos\frac{2\pi H_{Tx}H_{Rx}}{\lambda D}}{D^2}\right) = 0$$

$$\Rightarrow \frac{2\pi H_{Tx}H_{Rx}}{\lambda D}\tan\frac{2\pi H_{Tx}H_{Rx}}{\lambda D} = 2$$

$$\Rightarrow D \approx \frac{\sqrt{2}\pi H_{Tx}H_{Rx}}{\lambda} \qquad (56)$$

The above equation thus determines the position of the last maxima and hence can be used as criteria for the transition of the near-field to the far-field behavior for the radial component of the electric field. It is to be noted that the transition is 0.707 times earlier than the case of the vertical dipole above PEC as determined by Eqn. 18.

Fig.26 below summarizes the z-component and the radial component of the electric field due to a radiating dipole above PEC ground and urban soil characterized by relative permittivity of 4.0 and conductivity of 2e-4 mhos. The red line and the blue line shows the electric field due to the vertical dipole over the PEC ground and urban soil respectively, for the transmitter and the observed field position at a height of 10m and 2m above the ground. The solid line indicates the z-component of he electric field while the dotted component indicates the radial component of the electric field. The nulls and the peaks are more prominent in the case of PEC ground than in the case of urban ground.

Fig. 27 (a) and (b) below shows the magnitude of the z-component and the radial component of the electric fields due to a vertical dipole placed 10m above an imperfectly conducting ground of conductivity 2e-4 mhos but for different relative permittivity of the ground. Though there is some difference in the fields for different grounds, the position where the far-field characteristics takes over the near-field variation as determined by the position of the last null and the maxima seems to be independent up to the first order of the characteristics of the ground. This validates the approximate formulae like Eqns.50 and 55 used for the analysis and hence the discussions thereof.

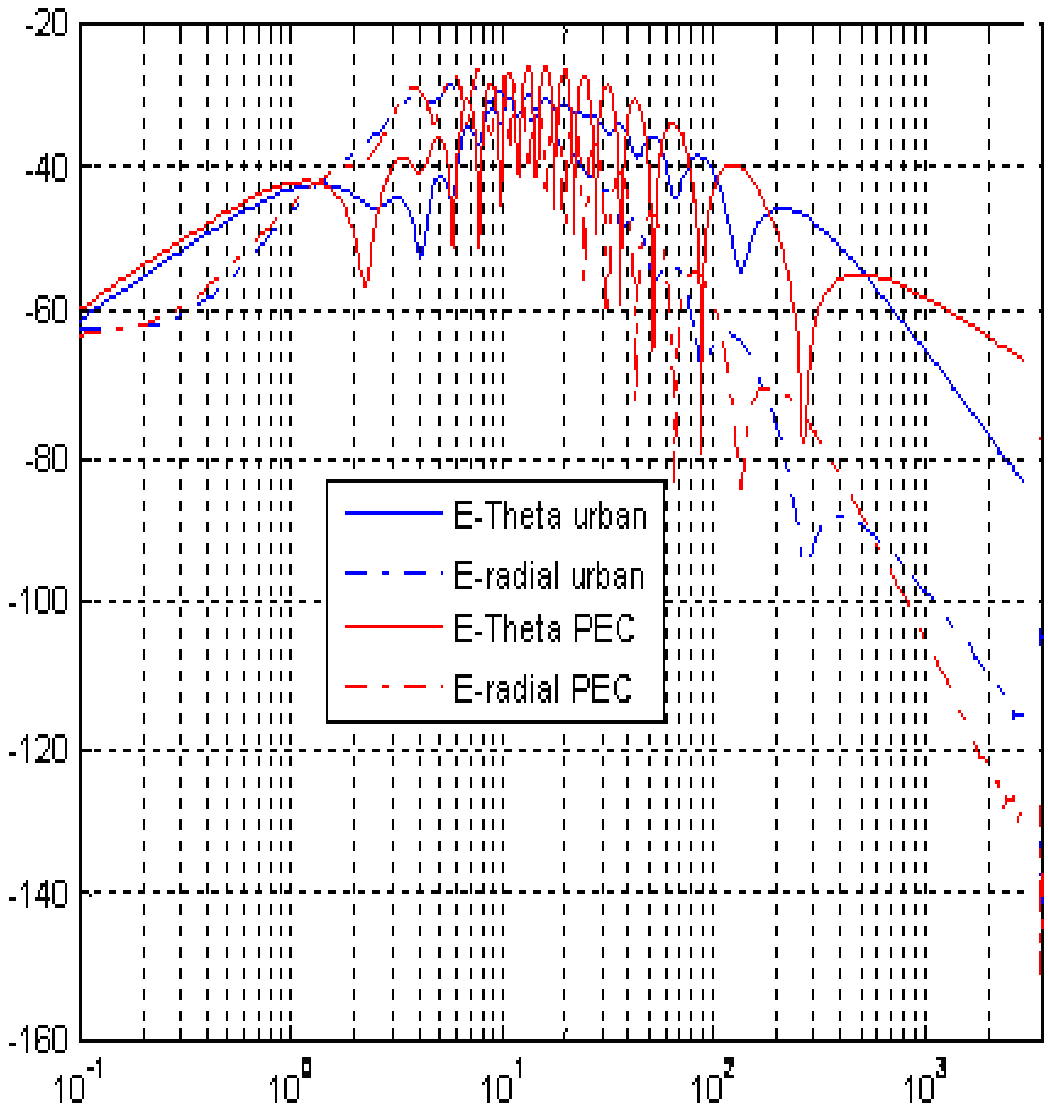

Figure 26: Comparison of the z-component of the Electric field due to a vertically oriented half-wave dipole placed 10m above urban ground of relative permittivity = 4.0, and with a conductivity of σ = 2e-4 mhos and above PEC ground. The field is observed 2m above the ground.

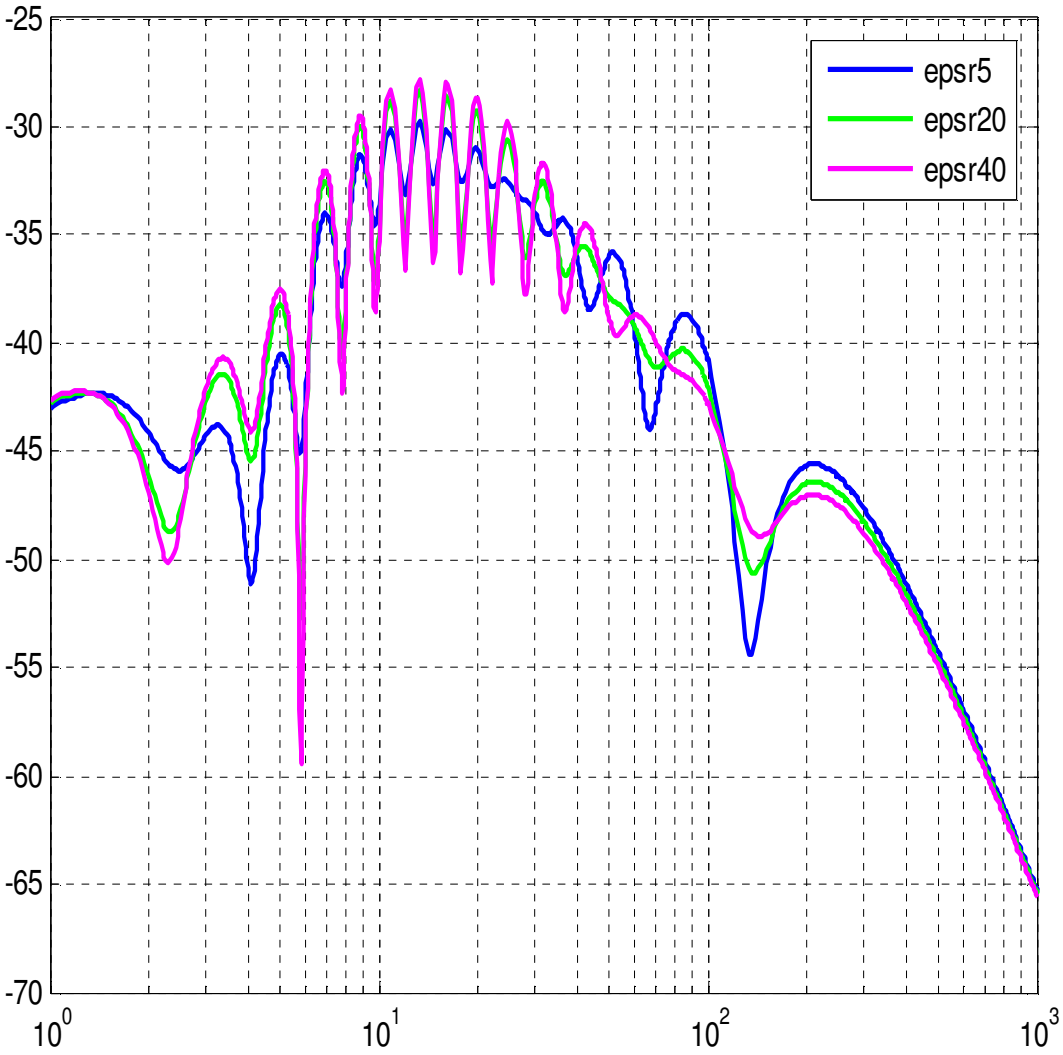

Figure 27 a: Comparison of the z-component of the Electric field due to a vertically oriented half-wave dipole placed 10m above imperfectly conducting ground of conductivity of σ = 2e-4 and various dielectric constant of the soil. The field is observed 2m above the ground.

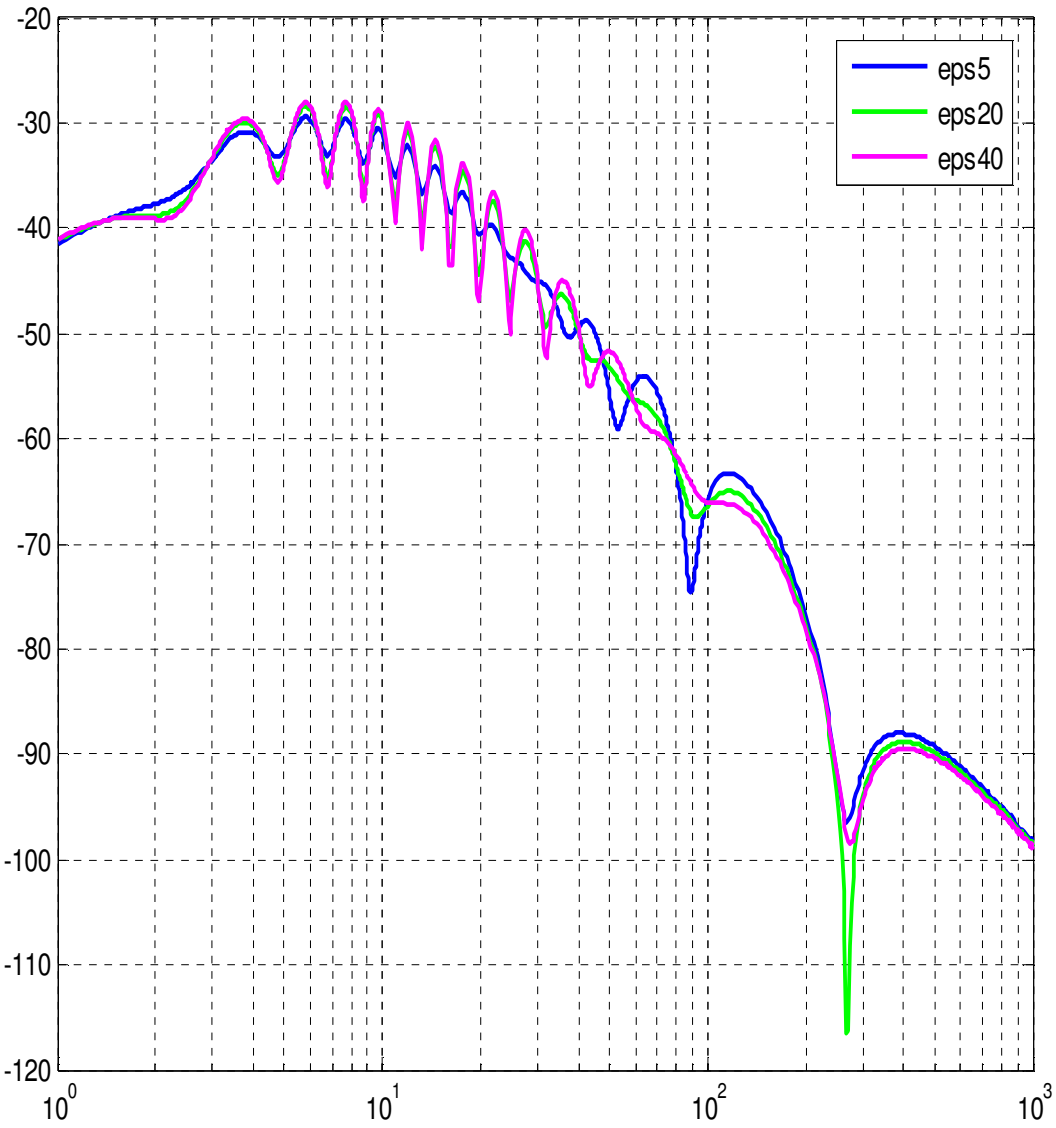

Figure 27 b: Comparison of the radial-component of the Electric field due to a vertically oriented half-wave dipole placed 10m above imperfectly conducting ground of conductivity of σ = 2e-4 and various dielectric constant of the soil. The field is observed 2m above the ground.

3.3 Horizontal Dipole above imperfectly conducting ground

We now consider the horizontally oriented Hertzian dipole over the real ground. The dipole is oriented parallel to the X-axis. This case was first solved by Hörschelman [1911], one of Sommerfeld's students. The Hertz vector potential in this case is both along the X and the Z-direction and is given as,

$$\Pi_x = -\frac{e^{jk_1R_1}}{R_1} + \frac{e^{jk_1R_2}}{R_2} - \int_{\lambda=0}^{\lambda=\infty} \lambda\, d\lambda\; J_o(\lambda\rho)\; \frac{2}{l+m} e^{-(z_a+z)l} \tag{57 a}$$

$$\Pi_z = -\cos\phi \int_{\lambda=0}^{\lambda=\infty} \lambda^2\, d\lambda\; J_o'(\lambda\rho) \frac{2\left(k_2^2 - k_1^2\right)}{\left(l+m\right)\left(k_2^2 l + k_1^2 m\right)} e^{-(z_a+z)l} \tag{57 b}$$

As seen in Eqn. 47, calculation of the fields requires us to compute the gradient of the divergence of the Hertz Potential. The divergence of the Hertz vector potential can be written according to Wise [1929] as,

$$\nabla.\Pi = \frac{\partial}{\partial x}\Pi_x + \frac{\partial}{\partial z}\Pi_z$$

$$= -\frac{\partial}{\partial x}\left[\frac{e^{jk_1R_1}}{R_1} - \frac{e^{jk_1R_2}}{R_2} + \int_{\lambda=0}^{\lambda=\infty} \lambda\, d\lambda\; J_o(\lambda\rho)\; \frac{2}{l+m} e^{-(z_a+z)l} \right]$$
$$+ \cos\phi \int_{\lambda=0}^{\lambda=\infty} \lambda^2\, d\lambda\; J_o'(\lambda\rho) \frac{2\left(k_2^2 - k_1^2\right)l}{\left(l+m\right)\left(k_2^2 l + k_1^2 m\right)} e^{-(z_a+z)l}$$

$$= -\frac{\partial}{\partial x}\left[\frac{e^{jk_1R_1}}{R_1} - \frac{e^{jk_1R_2}}{R_2} + \int_{\lambda=0}^{\lambda=\infty} \lambda\, d\lambda\; J_o(\lambda\rho)\; \frac{2}{l+m} e^{-(z_a+z)l} \right]$$
$$+ \frac{\partial}{\partial x}\left[\int_{\lambda=0}^{\lambda=\infty} \lambda\, d\lambda\; J_o(\lambda\rho) \frac{2\left(k_2^2 - k_1^2\right)l}{\left(l+m\right)\left(k_2^2 l + k_1^2 m\right)} e^{-(z_a+z)l} \right]$$

$$= -\frac{\partial}{\partial x}\left[\frac{e^{jk_1R_1}}{R_1} - \frac{e^{jk_1R_2}}{R_2} + \int_{\lambda=0}^{\lambda=\infty} \lambda\, d\lambda\; J_o(\lambda\rho)\; \frac{2k_1^2}{\left(k_2^2 l + k_1^2 m\right)} e^{-(z_a+z)l}\right] \tag{58}$$

Using Eqn. 48, the Electric Field along the z-direction can now be given as,

$$E_z = k_1^2 \Pi_z - \frac{\partial^2}{\partial z\, \partial x}\left[\frac{e^{jk_1R_1}}{R_1} - \frac{e^{jk_1R_2}}{R_2} + \int_{\lambda=0}^{\lambda=\infty} \lambda\, d\lambda\; J_o(\lambda\rho)\; \frac{2k_1^2}{\left(k_2^2 l + k_1^2 m\right)} e^{-(z_a+z)l}\right]$$

$$= -k_1^2 \cos\phi \int_{\lambda=0}^{\lambda=\infty} \lambda^2\, d\lambda\; J_o'(\lambda\rho) \frac{2\left(k_2^2 - k_1^2\right)}{(l+m)\left(k_2^2 l + k_1^2 m\right)}\; e^{-(z_a+z)l}$$
$$- \frac{\partial^2}{\partial z\, \partial x}\left[\frac{e^{jk_1R_1}}{R_1} - \frac{e^{jk_1R_2}}{R_2} + \int_{\lambda=0}^{\lambda=\infty} \lambda\, d\lambda\; J_o(\lambda\rho)\; \frac{2k_1^2}{\left(k_2^2 l + k_1^2 m\right)} e^{-(z_a+z)l}\right]$$

$$= -k_1^2 \cos\phi \frac{\partial^2}{\partial z\, \partial \rho} \int_{\lambda=0}^{\lambda=\infty} \lambda\, d\lambda\; J_o(\lambda\rho) \frac{2\left(k_2^2 - k_1^2\right)}{(l+m)\left(k_2^2 l + k_1^2 m\right)} \frac{e^{-(z_a+z)l}}{(-l)}$$
$$- \cos\phi \frac{\partial^2}{\partial z\, \partial \rho}\left[\frac{e^{jk_1R_1}}{R_1} - \frac{e^{jk_1R_2}}{R_2} + \int_{\lambda=0}^{\lambda=\infty} \lambda\, d\lambda\; J_o(\lambda\rho)\; \frac{2k_1^2}{\left(k_2^2 l + k_1^2 m\right)} e^{-(z_a+z)l}\right]$$

$$= -\cos\phi \frac{\partial^2}{\partial z\, \partial \rho}\left[\frac{e^{jk_1R_1}}{R_1} - \frac{e^{jk_1R_2}}{R_2} - V\right] \tag{59}$$

where V is as given in Eqn. A-9. Substituting the approximate value of V as given in Eqn. A-25 we get,

$$E_z \approx -\cos\phi \frac{\partial^2}{\partial z\, \partial \rho}\left[\frac{e^{jk_1R_1}}{R_1} + \frac{e^{jk_1R_2}}{R_2} - \frac{2\, jn^2 e^{jk_1R_2}}{k_1 {R_2}^2}\right] \tag{60}$$

Thus we see that the horizontally oriented dipole along the X-direction radiates vertically polarized Electric fields, which has a cosine variation along azimuth. The maximum being along the axial X-direction i.e. along φ =0. Using Eqns.52 and 53, the Electric field along the X-direction is given as,

$$E_z \approx (z-z_a)\frac{\rho}{R_1}\left(k_1^{\,2}\frac{e^{jk_1R_1}}{R_1^{\,2}}\right)+(z+z_a)\frac{\rho}{R_2}\left(k_1^{\,2}\frac{e^{jk_1R_2}}{R_2^{\,2}}\right)$$

$$\approx 2k_1^{\,2}e^{jk_1\frac{(z^2+z_a^{\,2})}{2\rho}}\frac{e^{jk_1\rho}}{\rho^2}\left[z\cos\left(k_1\frac{zz_a}{\rho}\right)+jz_a\sin\left(k_1\frac{zz_a}{\rho}\right)\right] \qquad (61)$$

Figure 28 below plots the E-z component of the electric field at a height of 2m above the ground along the end-fire direction i.e., along φ =0 of a horizontally oriented half-wave dipole located 10m above the ground. The blue line corresponds to the field calculated using AWAS. The red line corresponds to the field calculated using the above Eqn. 61. It can be seen that after around 30m from the transmitter, the fields calculated using the above approximate formulae and the Sommerfeld integral based numerical calculation yields almost similar results. The peaks and the nulls appear in similar positions and the far-field roll-off almost overlay with each other. In this case the far-field roll off is not simple as has been discussed before in other situations. Since the position of the transmitter (z_a) is generally larger than the position of the field observation point (z), the approximation given by the second part of Eqn. 61 assumes more significance. This can be seen by the green curve in Figure 28 which plots the second part with sinusoidal variation of Eqn. 61, while the yellow curve in Figure 28 corresponds to the first part

with co-sinusoidal variation only. We see that the green curve agrees very well with the actual numerical result in the very near-field and the radiating near-field zone of the antenna where we see sinusoidal variation of the field. The position characterizing the transition of the near to far field as given by the last null and the last maxima can thus be obtained by the second part of the Eqn. 61. The far-field roll-off immediately after the transition follows $1/R^3$ decay. After sufficient distance away from the transmitter the $1/R^2$ decaying first part of Eqn. 60 as shown by the yellow curve in Figure 29, takes over the $1/R^3$ decaying second part after which the magnitude of the far-field decays as $1/R^2$.

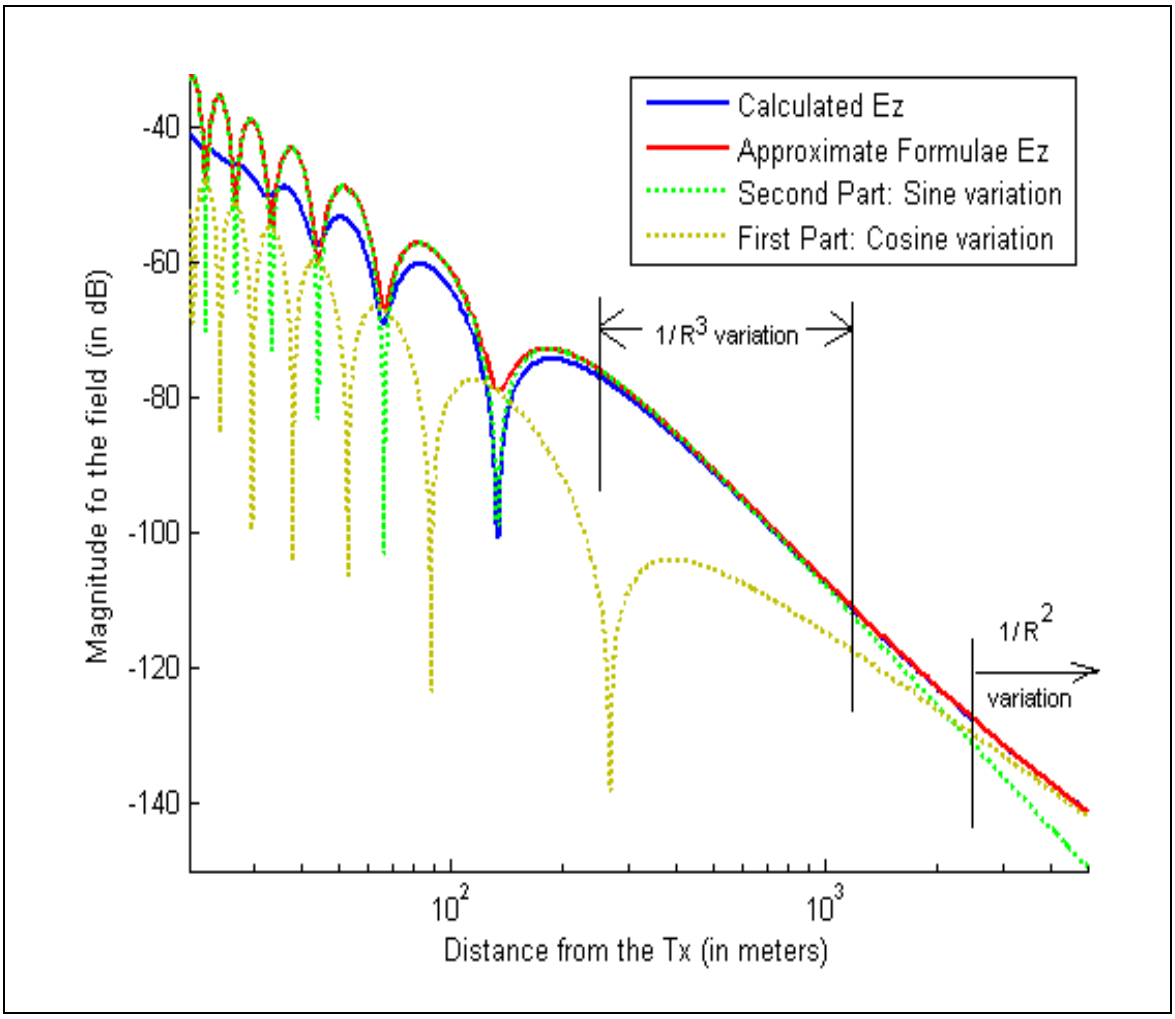

Figure 28: The *z*-component of the electric field due to a horizontally oriented dipole placed 10 m above urban soil and the field is observed 2 m above the ground.

The Eφ-component of the Electric field is given as,

$$E_\varphi = k_1^2\Pi_\varphi - \frac{1}{\rho}\frac{\partial^2}{\partial\varphi\partial x}\left[\frac{e^{jk_1R_1}}{R_1} - \frac{e^{jk_1R_2}}{R_2} + \int_{\lambda=0}^{\lambda=\infty}\lambda d\lambda\, J_o(\lambda\rho)\,\frac{2k_1^2}{\left(k_2^2 l + k_1^2 m\right)}e^{-(z_a+z)l}\right]$$

$$= k_1^2\Pi_x(-\sin\varphi) - \frac{1}{\rho}\frac{\partial}{\partial\varphi}\cos\varphi\frac{\partial}{\partial\rho}\left(\frac{e^{jk_1R_1}}{R_1} - \frac{e^{jk_1R_2}}{R_2} + \int_{\lambda=0}^{\lambda=\infty}\lambda d\lambda\, J_o(\lambda\rho)\,\frac{2k_1^2}{\left(k_2^2 l + k_1^2 m\right)}e^{-(z_a+z)l}\right)$$

$$= -\sin\varphi\left(k_1^2\Pi_x - \frac{1}{\rho}\frac{\partial}{\partial\rho}\left[\frac{e^{jk_1R_1}}{R_1} - \frac{e^{jk_1R_2}}{R_2} + \int_{\lambda=0}^{\lambda=\infty}\lambda d\lambda\, J_o(\lambda\rho)\,\frac{2k_1^2}{\left(k_2^2 l + k_1^2 m\right)}e^{-(z_a+z)l}\right]\right) \tag{62}$$

The Hertz potential along the X-direction is given as in Eqn.55. Using the identity given in Eqn. A-1, the third term involving the integration can be modified as,

$$H = \int_{\lambda=0}^{\lambda=\infty}\lambda d\lambda\, J_o(\lambda\rho)\,\frac{2}{l+m}e^{-(z_a+z)l}$$

$$= \int_{\lambda=0}^{\lambda=\infty}\lambda d\lambda\, J_o(\lambda\rho)\left(2 - \frac{2m}{l+m}\right)\frac{e^{-(z_a+z)l}}{l}$$

$$=2\frac{e^{jk_1R_2}}{R_2}-\int_{\lambda=0}^{\lambda=\infty}\lambda d\lambda\, J_o(\lambda\rho)\,\frac{2m}{l+m}\frac{e^{-(z_a+z)l}}{l} \tag{63}$$

Following the same procedure as used in the approximation of *V* in the Appendix-A, we can obtain an approximation to the second integral in Eqn. 62. Thus Eqn. 62 can now be approximated as,

$$H \approx 2\frac{e^{jk_1R_2}}{R_2}-2\frac{e^{jk_1R_2}}{R_2}\left(1-\frac{j}{k_1R_2}\right)$$

$$= 2j\frac{e^{jk_1R_2}}{k_1R_2^2} \tag{64}$$

Using Eqn. 63, the Hertz vector potential along the X-direction as given in Eqn.55 can be approximated as,

$$\Pi_x=-\frac{e^{jk_1R_1}}{R_1}+\frac{e^{jk_1R_2}}{R_2}-2j\frac{e^{jk_1R_2}}{k_1R_2^2} \tag{65}$$

Since the contribution of the other terms for E_φ in Eqn. 61 are of $O(1/R_1^2)$, we can neglect them and the primary contribution can be assumed to be from Π_x . Hence the horizontally polarized Electric field along the Y-direction i.e. at $\varphi = 90^o$ due to the horizontally oriented dipole over the imperfect earth is given as,

$$E_\varphi = k_1^2\left(\frac{e^{jk_1R_1}}{R_1}-\frac{e^{jk_1R_2}}{R_2}\right) \tag{66}$$

$$\approx -2jk_1^2 e^{jk_1\frac{(z^2+z_a^2)}{2\rho_0}} \frac{e^{jk_1\rho}}{\rho} \sin\left(k_1 \frac{z z_a}{\rho}\right) \tag{67}$$

Figure 29 below plots the Phi-component of the electric field for a horizontally oriented transmitting dipole antenna along the X-direction at a frequency of 1 GHz. The antenna is placed 10 m above an imperfectly conducting ground. A relative permittivity ε_r = 4.0 and conductivity of $\sigma = 2 \times 10^{-4}$ mhos/m representing the properties of a typical urban ground. Electric fields are calculated at a height of 2 m from the ground along the Y-direction i.e. at $\varphi = 90^o$.

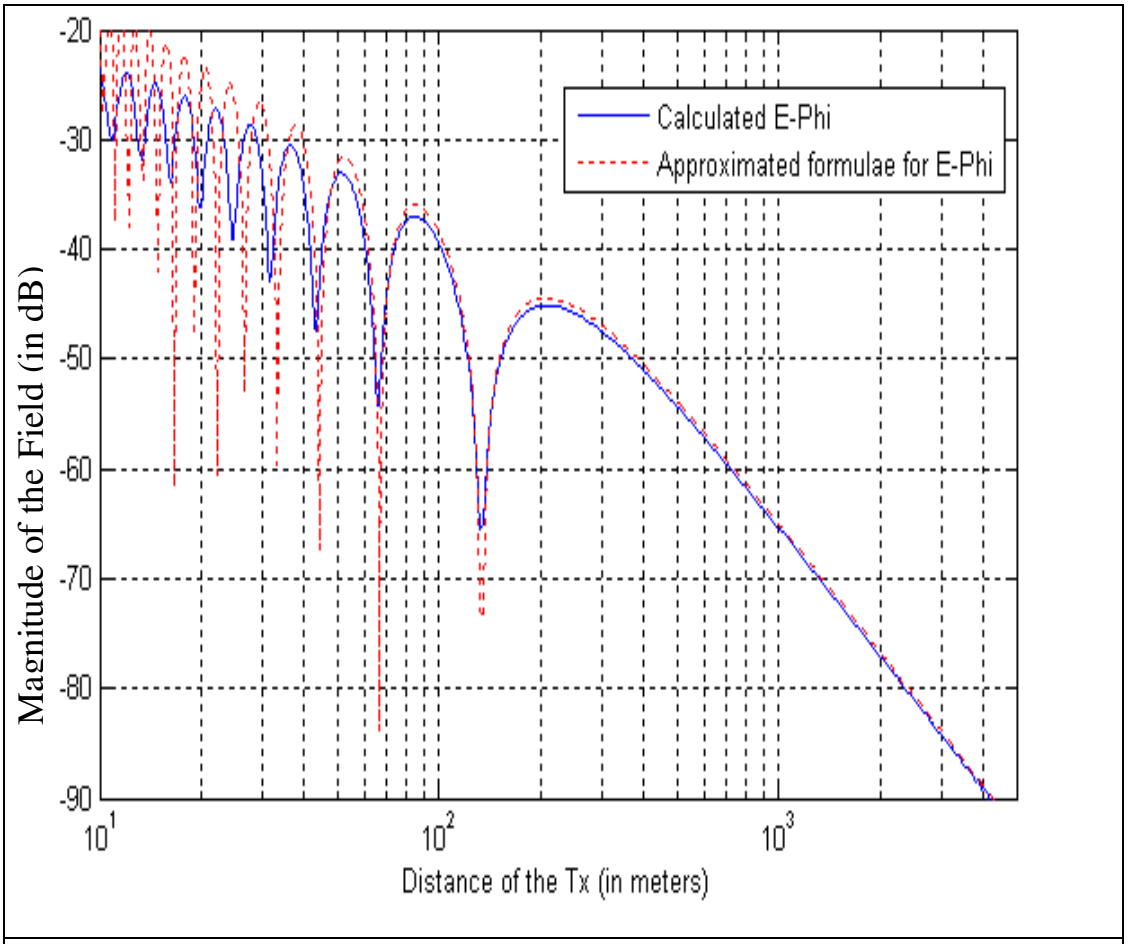

Figure 29: Comparison of the *Phi*-component of the electric field due to a

horizontally oriented Hertzian dipole using Eqns. 67 and a half-wave dipole when the transmitting antenna is placed 10 m above urban soil and the field is observed 2 m above an urban ground of relative permittivity of 4.0

The deep-blue line indicates the E_φ component of the electric field calculated using AWAS. The red dotted line indicates the E_φ component of the electric field calculated using the above Eqn. (67). As in the case of the vertically oriented dipole antenna, we see for distances greater than approximately five times the height of the transmitter, the approximate formula of (67) matches with the simulation results. The predicted position of the last null is also given by Eqn. (24) as in the case of the vertically oriented dipole above the imperfectly conducting ground. We see from Fig. 29 that the predicted position of the last null agrees well with the simulated data carried out using the more accurate Sommerfeld formulation.

Figure 30 below plots the Phi-component of the electric field due to a horizontally oriented dipole along the X-direction above an urban ground and a PEC ground. The blue line shows the field above the urban ground and the red line shows the field above a PEC ground along the Y-direction i.e. at $\varphi = 90^o$. It is interesting to note that the field above the PEC and the imperfectly conducting ground varies similarly with almost similar positions in the location of the nulls and the peaks in the field distribution. The only difference is that the variation is more pronounced as the relative permittivity of the ground increases, the maximum being when the ground is PEC. In the far-field, the field decays as $1/R^2$ for both the cases.

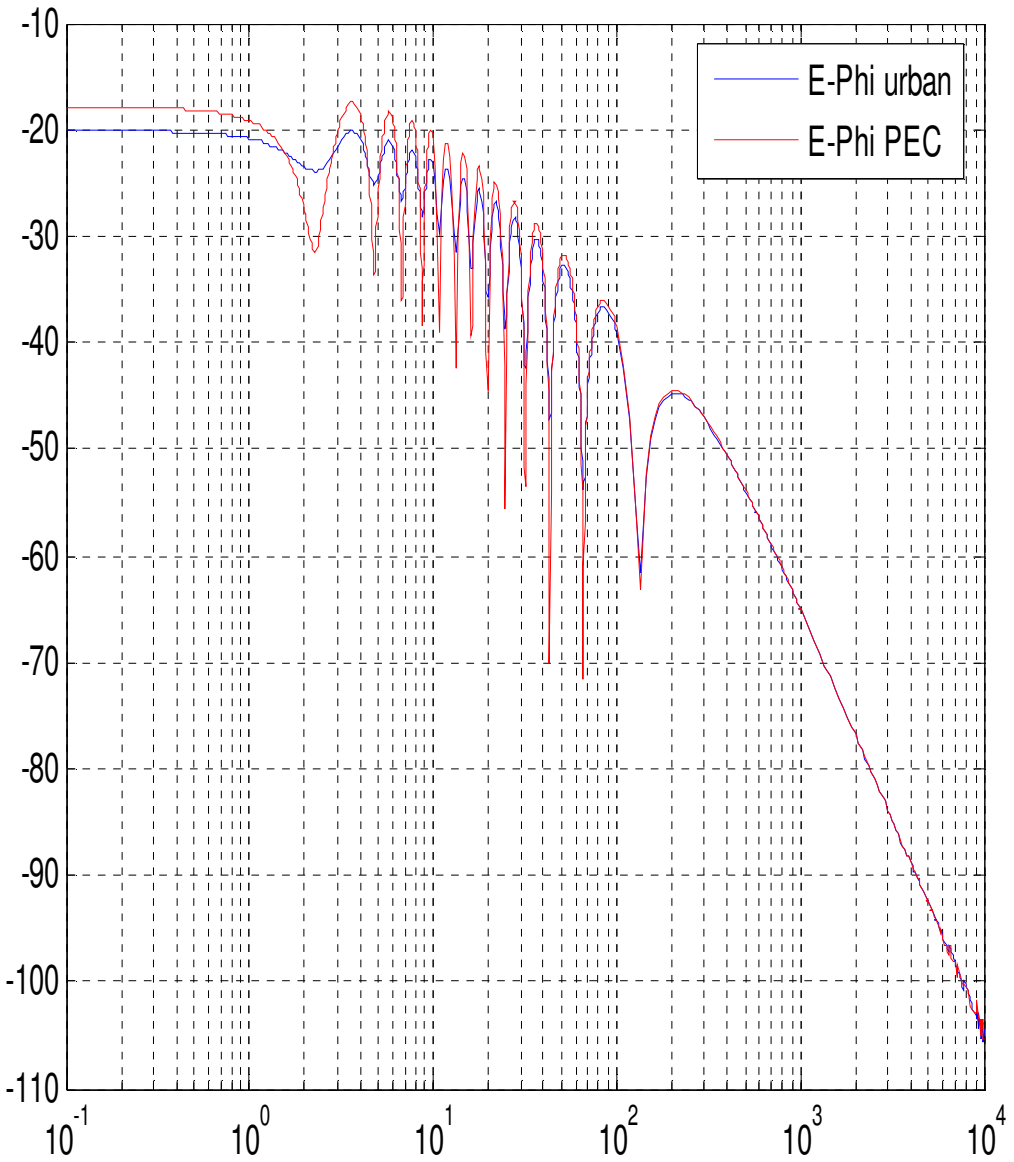

Figure 30: Comparison of the phi-component of the electric field due to a horizontally oriented half-wave dipole placed 10 m above an urban ground of relative permittivity of 4.0, and a conductivity of σ = 2e-4 and above a PEC ground. The field is observed at a height of 2 m from the ground.

3.3 Conclusions

Figure 31 (a) plots the comparisons of the various components of the fields due to the vertically oriented and the horizontally oriented dipole antennas above the imperfectly conducting ground plane at the frequency of 1GHz. The horizontally oriented dipole antenna is along the X-direction. In both the cases, the antenna is placed 10 m above an imperfectly conducting ground of relative permittivity $\varepsilon = 4.0$ and conductivity of $\sigma = 2 \times 10^{-4}$ mhos/m representing the properties of a typical urban ground. Electric fields are calculated at a height of 2 m from the ground.

The blue line corresponds to the Z-component of the electric field due to the vertically oriented dipole antenna and the red line corresponds to the Phi-component of the electric field due to the horizontally oriented dipole antenna along the Y-direction i.e. along $\varphi = 90^{o}$. We see that in the very near-field of the antenna the magnitude of the Phi-component due to the horizontally oriented antenna is larger than the Z-component due to the vertically oriented antenna. The variation in the radiating near-field of the antenna is larger in the case of the horizontally oriented antenna than in the vertically oriented antenna, though both exhibit the sinusoidal variation.

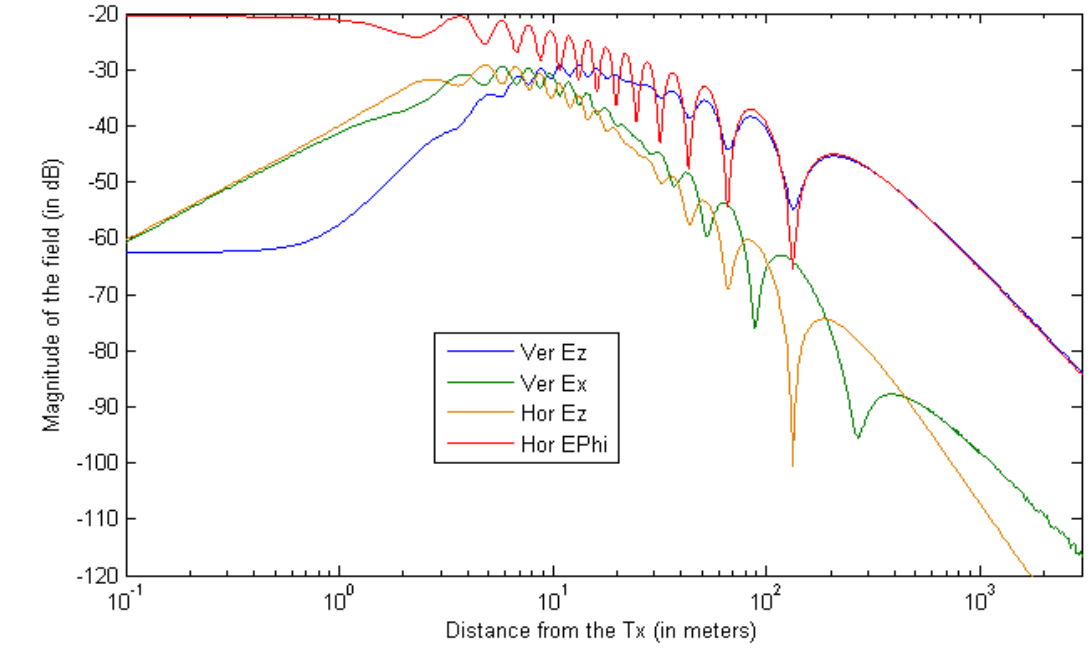

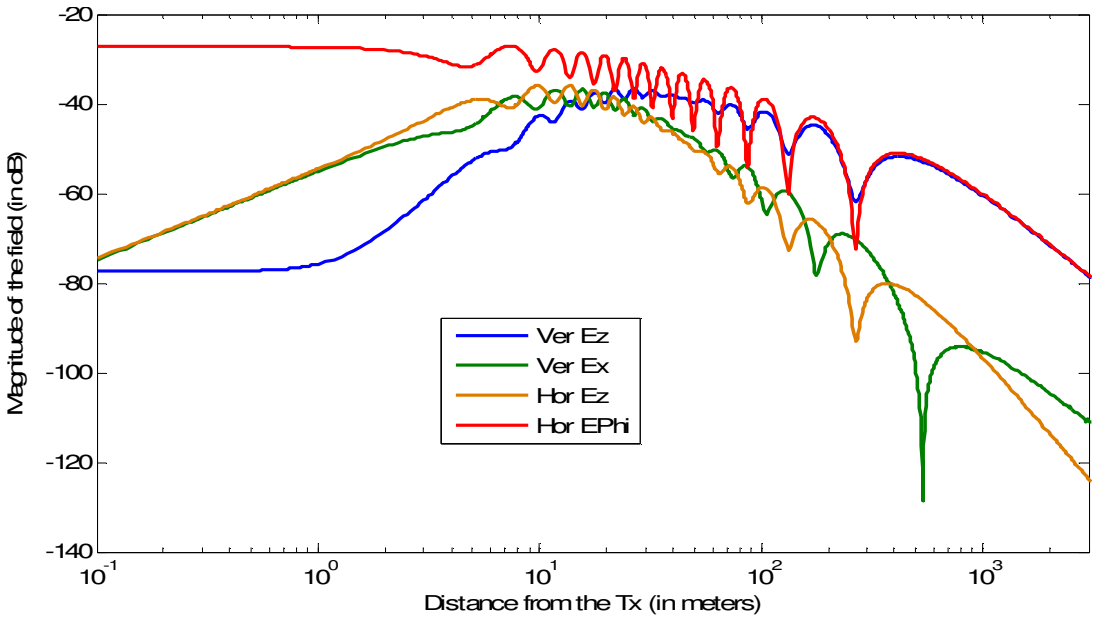

Figure 31: Various components of the electric field due to vertically and horizontally oriented dipole placed 10m (top fig.) and 20 m (bottom fig.) above the urban ground.

The field is observed at 2m ht.

The far-field behavior of the field components due to both the antennas are however similar and follow a $1/R^2$ decay. The green line corresponds to the radial component of the field due to the vertically oriented antenna. It is though considerably smaller than the Z-component of the field by around 32 dB. This difference is constant in the far-field of the antenna in this case unlike the case of the vertically oriented dipole antenna above a PEC ground, where the radial component decreases by $1/R^3$. The brown line indicates the Z-component of the electric field due to a horizontally oriented dipole antenna along the end-fire direction i.e. along $\varphi = 0^o$. As discussed before the far-field in this case first rolls-off as $1/R^3$, but after considerable distance away from the transmitter, the field decays as $1/R^2$. The magnitude of the field component in the far-field is however much less compared to all the other three components of the field as discussed above. With the exception of the radial component of the electric field due to the vertically oriented dipole antenna, the transition position of the near-field zone to the radiating far-field zone for all the field components are almost the same as given by Eqn. 33, 36 or 37 based on the different criterion. For the radial component of the vertically oriented antenna the field exhibits a co-sinusoidal variation instead of the sinusoidal variation and the transition position is almost twice the distance compared to all the other cases as given by Eqn. 15, 18 or 16 respectively for the different criterion as discussed before.

Figure 31 (b) plots the similar comparisons of the various components of the fields due to the vertically oriented and the horizontally oriented dipole antennas located 20 m above the imperfectly conducting urban ground plane. Electric fields are calculated at a

height of 2 m from the ground. We notice that almost half the entire range of a typical cellular communication zone falls within the near-field region of the antenna. This essentially stimulates us to make some thought regarding the optimum positioning of the antenna near the ground such that most of the communication zone within a cell lies within the radiating far-field region of the antenna.

4. CONCLUSIONS

In this dissertation, few topics related to the near-field and far-field behavior of a vertically oriented and a horizontally oriented antenna above a ground plane are discussed. Some specific expressions have been derived which correspond to this transition region, based on different criterions, for both the horizontal and the vertical dipole case. These expressions are validated by simulations. For both the vertically and the horizontally oriented antennas above the ground plane, the very near-field is almost the same and is determined by the position where the wave impedance approaches free space impedance, and the phase of the wave impedance approaches zero. The transition position is linearly varying with the height of the Transmitting antenna above the PEC ground plane. Beyond this point there is negligible reactive energy stored and one is in the radiative near-field of the antenna. As one move further ahead the wave sphericity condition (where the magnitude of the field decays monotonously with the distance) determines the transition from the radiative near-field to the radiating far-field of the antenna. This transition position also changes linearly with the height of the transmitter above the ground plane. However for the vertical antenna this distance is almost double the distance than for the horizontal antenna.

In the near-field region of the antenna smart antenna techniques like beam-forming are difficult to achieve. The traditionally used spatial processing gain for an M-element array as commonly used in Wireless Communication literature as in Eq. 5.11 of Liberti and Rappaport [1999] does not quite hold true in the near-field region of antennas over a ground plane where the field varies rapidly due to the interference between the

source and the image which is often labeled as fast fading in traditional wireless communication text books as in Jakes [1974]. Thus for a reliable and efficient communication one should take care of this far-field criterion and then approach a system design for optimum positioning of the transmitting and receiving antenna from a Maxwellian framework.

Figure 32 and 33 shows the variation of the received field due to different heights of the transmitter above the urban ground. We see that in the far-field regime the magnitude of the field increases with the height of the transmitting antenna above the ground as predicted by Eqn. 50. Fig. 32 shows the field due to the transmitter height of 5 m, 10 m, 20 m, 100 m, and ½ Km from the ground for the operating frequency of 453 MHz, while Fig. 33 shows the field due to the same heights of the transmitter for the operating frequency of 1 GHz as discussed by Okumura [1968].

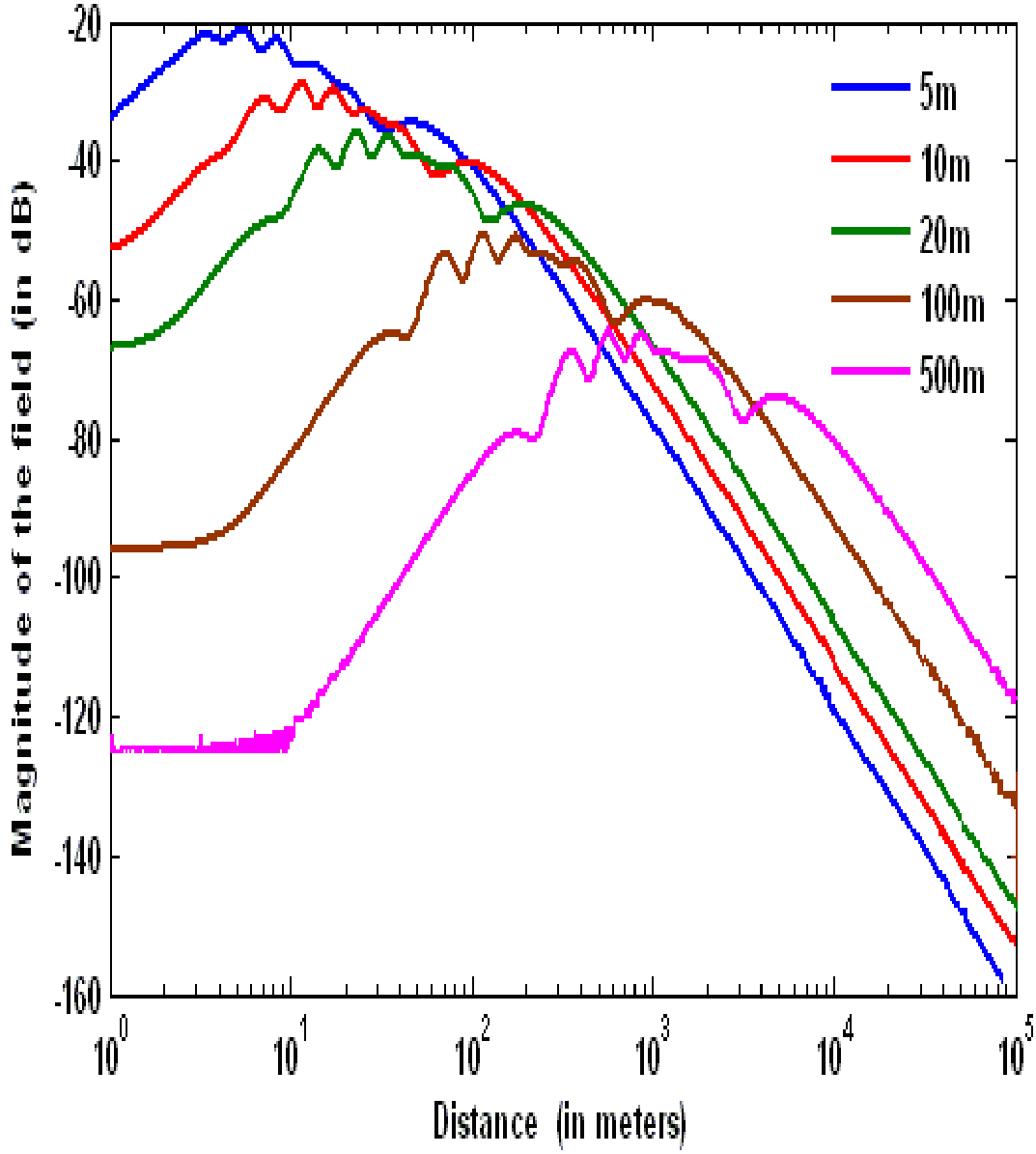

Figure 32: Variation of the magnitude of the Ez component of the Electric field from a half-wavelength dipole with distance. Freq 453 MHz (as in Okumura), Rx ht at 2m, and ground is urban soil of permittivity $\varepsilon_r = 4.0$, and with a conductivity of $\sigma = 2 \text{ X } 10^{-4}$.

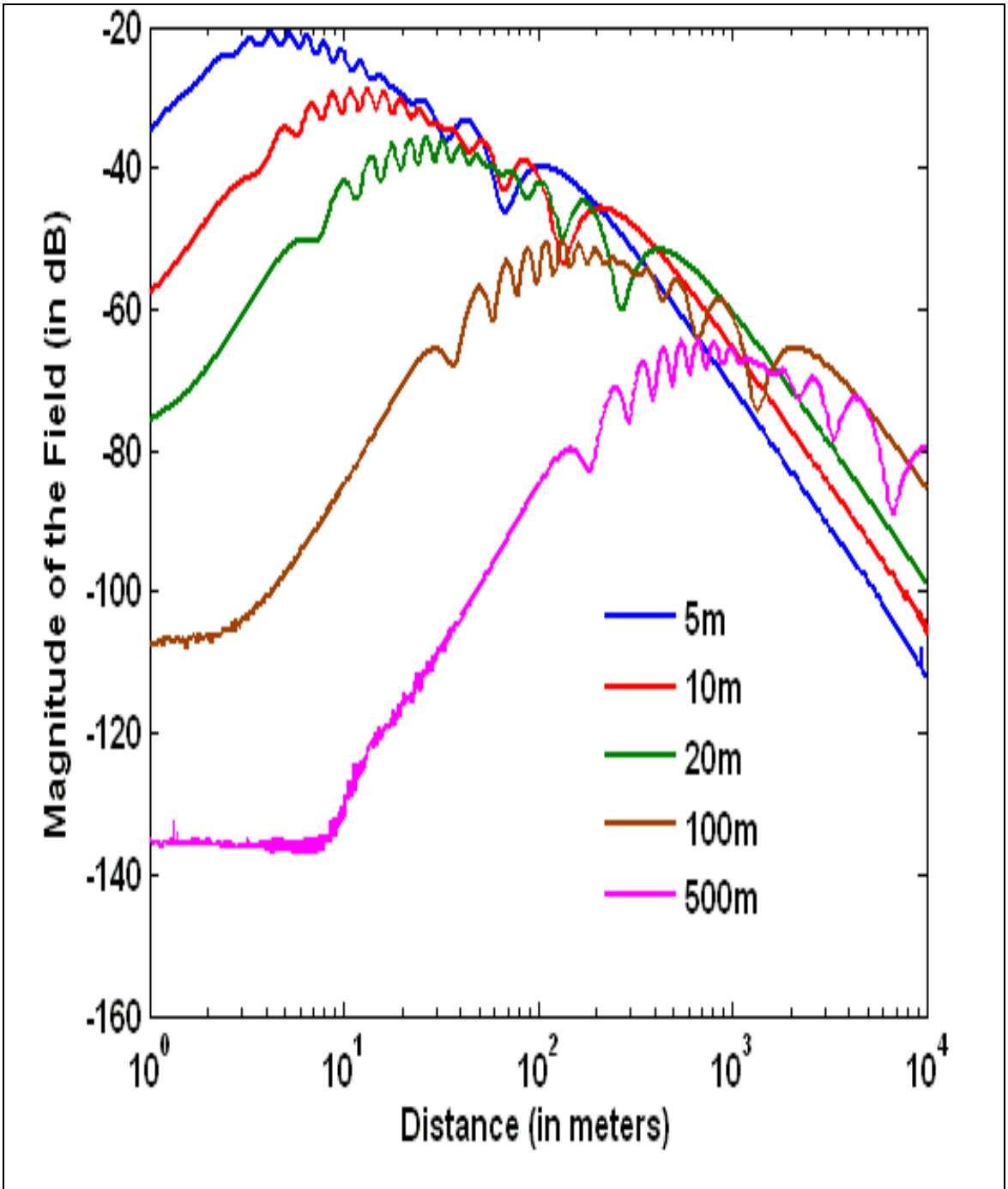

Figure 33: Variation of the magnitude of the Ez component of the Electric field from a half-wavelength dipole with distance. Freq 1000 MHz (as in Okumura), Rx ht at 2m, and ground is urban soil of permittivity $\varepsilon_r = 4.0$, and with a conductivity of $\sigma = 2 \text{ X } 10^{-4}$.

The increase in the magnitude of the field with the increase in the height of the transmitter is referred to as height-gain in the common literature. The main objective of this dissertation is to emphasize the fact that the position where the far-field of the antenna takes over the near-field also increases linearly with the height of the transmitting antenna. Thus one needs to judiciously position the transmitting antenna such that most of the operating region falls within the far-field of the antenna. Hence we cannot increase the height of the transmitting antenna arbitrarily. For example as seen in Fig. 32, the far-field starts at around 5 Km for the transmitting antenna placed at a height of 500 m above the ground. Since the cellular coverage is roughly within a radius of 3 Km, the whole region is mostly within the near-field of the antenna. Similarly for the antenna at a height of 100 m, the far-field starts around 1 Km, thus almost one third of the cellular operating area is in the near field of the antenna. In summary, the height-gain in the fields reflected in the far field does not occur in the near field regions, where most cellular systems operate. This erroneous conclusion of height gain was arrived from Okamura's experimental data for measuring field strength which was only for the far field region, in the city of Tokyo, from transmitting antennas located at various heights on top of Mount Fuji.

A.1 APPENDIX A

In order to obtain some simple expressions for the position of the last null indicating the transition from the near-field to the far-field of the radiating antenna Eqn. 43 needs some simplification. We first need to make some approximations to get rid of the Bessel function of order 0, $J_0(\lambda\rho)$ in Eqn. 43. The way to get rid of the Bessel function is to use the following representation of the point source in free space given by Sommerfeld [1949],

$$\frac{e^{jkr}}{r} = \int_{\lambda=0}^{\lambda=\infty} \lambda \, d\lambda \; J_o(\lambda\rho) \frac{e^{-|z_0| l}}{l} \tag{A-1}$$

with *l* and *r* given by,

$$l = \sqrt{\lambda^2 - k^2} \tag{A-2}$$

$$r = \sqrt{\rho^2 + z_0^2} \tag{A-3}$$

Using the relationship of the Fourier-Bessel transform as in Watson [1944],

$$f(\rho) = \int_0^{\infty} \sigma \, d\sigma \; \varphi(\sigma) \, J_0(\sigma\rho) \tag{A-4}$$

$$\varphi(\sigma) = \int_0^{\infty} \rho \, d\rho \; f(\rho) \, J_0(\sigma\rho)$$

we obtain the inversion formulae of Eqn. A-1 as ,

$$\frac{e^{-|z_0| l}}{l} = \int_{\rho=0}^{\rho=\infty} \rho \; d\rho \; J_o(\lambda\rho) \frac{e^{jkr}}{r} \tag{A-5}$$

Eqn. A-1 and A-5 are the main tools that have been used by several researchers to transform the Bessel function in Eqn. 43 and obtain various asymptotic expansions valid at different regions of the half-space.

An ingenious transformation of the rational polynomial term containing l and m as suggested by VanDerPol [1935], facilitates the application of the above mentioned identities to reduce Eqn. 43 in much simpler form. Since both k_1^2 and k_2^2 lie in the first quadrant of the complex plane hence both l and m as defined by Eqns. 44 and 45 lie in the fourth quadrant of the complex plane for all real values of λ valid within the range of integration of Eqn. 43. $k^2_2.l$ and $k^2_1.m$ lies either in the first or the fourth quadrant and hence has the real part positive. Thus we have the following convergent integral and hence the identity,

$$\int_0^\infty e^{-(k_2^2 l + k_1^2 m)\zeta}\, d\zeta = \frac{1}{k_2^2 l + k_1^2 m} \tag{A-6}$$

The second term in Eqn. 43 can then be transformed as,

$$\frac{1}{l}\frac{k_1^2 m}{k_2^2 l + k_1^2 m} = k_1^2 \frac{m}{l}\int_0^\infty e^{-(k_2^2 l + k_1^2 m)\zeta}\, d\zeta$$

$$= \frac{1}{k_1^2}\int_0^\infty \left[\left(\frac{e^{-k_2^2 l\zeta}}{l}\right)\cdot\frac{\partial^2}{\partial\zeta^2}\left(\frac{e^{-k_1^2 m\zeta}}{m}\right)\right] d\zeta \tag{A-7}$$

Using Eqns. A-6 and A-7 we can re-write the total Hertzian potential of Eqn. 41 as,

$$\Pi_1 = \frac{e^{jk_1 R_1}}{R_1} + \frac{e^{jk_1 R_2}}{R_2} + V \tag{A-8}$$

where V is given by,

$$V = -\frac{2}{k_1^2} \int_{\lambda=0}^{\lambda=\infty} \lambda \, d\lambda \; J_o(\lambda\rho) \int_{\zeta=0}^{\zeta=\infty} \left[\left(\frac{e^{-(z_a + z + k_2^2 \zeta) l}}{l} \right) . \frac{\partial^2}{\partial \zeta^2} \left(\frac{e^{-k_1^2 m \zeta}}{m} \right) \right] d\zeta \tag{A-9}$$

Since m is a function of λ, one can get rid of m using the inversion Eqn.A-5 as,

$$\frac{e^{-k_1^2 m \zeta}}{m} = \int_{\sigma=0}^{\sigma=\infty} \sigma \, d\sigma \; J_o(\lambda\sigma) \frac{e^{jk_2 \sqrt{(k_1^2 \zeta)^2 + \sigma^2}}}{\sqrt{(k_1^2 \zeta)^2 + \sigma^2}} \tag{A-10}$$

Thus V is given by the following triple integral,

$$V = \frac{2}{k_1^2} \int_{\zeta=0}^{\zeta=\infty} d\zeta \int_{\sigma=0}^{\sigma=\infty} \sigma d\sigma \frac{\partial^2}{\partial \zeta^2} \left(\frac{e^{jk_2 \sqrt{(k_1^2 \zeta)^2 + \sigma^2}}}{\sqrt{(k_1^2 \zeta)^2 + \sigma^2}} \right) \int_{\lambda=0}^{\lambda=\infty} \left[\lambda d\lambda \frac{e^{-(z_a + z + k_2^2 \zeta) l}}{l} J_o(\lambda\rho) . J_o(\lambda\sigma) \right] \tag{A-11}$$

Using the addition theorem for Bessel functions as in Watson [1944], we have,

$$J_0(\lambda \sqrt{\rho^2 + \sigma^2 - 2\rho\sigma\cos\varphi}) = \sum_{n=-\infty}^{n=\infty} J_n(\lambda\rho) J_n(\lambda\sigma) e^{jn\varphi} \tag{A-12}$$

Integrating Eqn.A-12 with respect to φ between [0,2π] we have,

$$J_0(\lambda\rho_0)J_0(\lambda\sigma)=\frac{1}{2\pi}\int_0^{2\pi} J_0(\lambda\sqrt{\rho_0^2+\sigma^2-2\rho_0\sigma\cos\varphi})d\varphi \tag{A-13}$$

Using Eqns.A-1 and A-13 we can thus write V of Eqn. A-11 as,

$$V=-\frac{1}{\pi k_1^2}\int_{\zeta=0}^{\zeta=\infty} d\zeta \int_{\sigma=0}^{\sigma=\infty} \sigma\, d\sigma\ \frac{\partial^2}{\partial\zeta^2}\left(\frac{e^{jk_2\sqrt{(k_1^2\zeta)^2+\sigma^2}}}{\sqrt{(k_1^2\zeta)^2+\sigma^2}}\right)\int_{\varphi=0}^{\varphi=2\pi} d\varphi\ \frac{e^{jk_1R'}}{R'} \tag{A-14}$$

where, R′ is given as,

$$R'=\sqrt{\rho^2+\sigma^2-2\rho\sigma\cos\varphi+(z_a+z+k_2^2\zeta)^2} \tag{A-15}$$

So, far the expressions for the Hertz vector potential have been exact. In order to calculate the field at a large distance away from the transmitter we make certain approximations to come up with some simple expressions. First we assume that the medium-1 (which in most cases is air medium) is lossless, i.e. k_1^2 is a real number. We can then substitute z' for $k_1^2\zeta$. Hence Eqn. A-14 becomes,

$$V=-\frac{1}{\pi}\int_{z=0}^{z=\infty} dz'\int_{\sigma=0}^{\sigma=\infty}\sigma\, d\sigma\int_{\varphi=0}^{\varphi=2\pi} d\varphi\ \frac{\partial^2}{\partial z'^2}\left(\frac{e^{jk_2\sqrt{z'^2+\sigma^2}}}{\sqrt{z'^2+\sigma^2}}\right)\frac{e^{jk_1R'}}{R'} \tag{A-16}$$

To facilitate the integration of Eqn. A-16 with respect to φ, we make certain approximations of R'. Observing the above equation we can obtain an insightful physical

explanation. The expression $\partial^2/\partial z'^2\left(e^{jk_2\sqrt{z'^2+\sigma^2}}\Big/\sqrt{z'^2+\sigma^2}\right)$ represents a wave spreading from the geometrical image A' in Fig. 24 with a velocity and absorption (k_2) belonging to the second medium, while each of the points of this second medium below the geometrical image A' sends secondary waves with a propagation constant k_1 belonging to the first medium. Now if the second medium is assumed to be quite lossy, i.e. k_2^2 have a great imaginary part, then due to high absorption, the wave will be rapidly attenuated. Thus only the immediate neighborhood (but below the level) of the geometrical image A', can then be considered to send the secondary waves to the observation point at B. Introducing $n^2 = k_2^2/k_1^2$, as the refractive index of the second medium with respect to the first medium, R' from Eqn. A-15 can be modified in the far zone of the antenna i.e. where $\rho \gg \sigma$ as,

$$R' \approx \sqrt{\rho^2 + (z_a + z + n^2 z')^2} \tag{A-17}$$

This facilitates the removal of the φ-dependence of R'. Substituting the value of R_2 in the above expression, and using the binomial series expansion we obtain,

$$R' \approx R_2 + \frac{n^4 z'^2}{2R_2} + \frac{n^2 z'(z_a + z)}{R_2} \tag{A-18}$$

Substituting the above Eqn. in Eqn. A-16, we can thus approximate V as,

$$V = -2\int_{z'=0}^{z'=\infty} dz' \frac{e^{jk_1 R'}}{R'} \int_{\sigma=0}^{\sigma=\infty} \sigma\, d\sigma \frac{\partial^2}{\partial z'^2}\left(\frac{e^{jk_2\sqrt{z'^2+\sigma^2}}}{\sqrt{z'^2+\sigma^2}}\right)$$

$$=-2\int_{z'=0}^{z'=\infty} dz' \frac{e^{jk_1R'}}{R'} \frac{\partial^2}{\partial z'^2}\left(\int_{\sigma=0}^{\sigma=\infty} d\left(\sqrt{z'^2+\sigma^2}\right) e^{jk_2\sqrt{z'^2+\sigma^2}}\right)$$

$$=-\frac{2}{jk_2}\int_{z'=0}^{z'=\infty} dz' \frac{e^{jk_1R'}}{R'} \frac{\partial^2}{\partial z'^2}\left(e^{jk_2\sqrt{z'^2+\sigma^2}}\Big|_{\sigma=0}^{\sigma=\infty}\right)$$

$$=\frac{2}{jk_2}\int_{z'=0}^{z'=\infty} dz' \frac{e^{jk_1R'}}{R'} \frac{\partial^2}{\partial z'^2} e^{jk_2z'}$$

$$=2\,jk_2\int_{z'=0}^{z'=\infty} dz' \frac{e^{jk_1\left(R_2+\frac{n^4z'^2}{2R_2}+\frac{n^2z'(z_a+z)}{R_2}+nz'\right)}}{R_2+\frac{n^4z'^2}{2R_2}+\frac{n^2z'(z_a+z)}{R_2}} \qquad \text{(A-19)}$$

where, the last term at $\sigma = \infty$ vanishes because k_2 lies in the first quadrant of the complex plane and hence has a negative real part in the exponent. Since the secondary sources are mostly concentrated near the image point for a lossy ground, Norton [1937] suggests that we can further approximate V for the observation point at large enough distance from the transmitter, by moving the amplitude variation of R' outside the integral taking care of only the phase variation.

Thus we obtain,

$$V \approx \frac{2\,jk_2e^{jk_1R_2}}{R_2}\int_{z'=0}^{z'=\infty} dz'\, e^{jk_1\left(\frac{n^4z'^2}{2R_2}+\frac{n^2z'(z_a+z)}{R_2}+nz'\right)}$$

$$=\frac{2\,jk_2e^{jk_1R_2}}{R_2}\int_{z'=0}^{z'=\infty} dz'\, e^{-(a^2z'^2+bz')}$$

$$= \frac{2\,jk_2 e^{jk_1 R_2 + \frac{b^2}{4a^2}}}{R_2} \int_{z'=0}^{z'=\infty} dz'\; e^{-(az' + \frac{b}{2a})^2} \tag{A-20}$$

By, change of variables we get,

$$V = \frac{j\sqrt{\pi}\, k_2 e^{jk_1 R_2 + \frac{b^2}{4a^2}}}{a R_2} erfc\left(b/2a\right) \tag{A-21}$$

where, *erfc* is the complementary error function is given by,

$$erfc(z) = \frac{2}{\sqrt{\pi}} \int_z^\infty e^{-t^2} dt \tag{A-22}$$

For sufficiently large z (i.e. $z \rightarrow \infty$) and $-3\pi/4 < \arg(z) < 3\pi/4$, there exists an asymptotic expansion of the complementary error function as given in Abramowitz and Stegun [1965] p. 298, Eq. 7.1.23 given by,

$$\sqrt{\pi}\, z e^{z^2} erfc(z) \approx 1 + \frac{-1}{2z^2} + \frac{1.3}{\left(2z^2\right)^2} + \frac{-1.3.5}{\left(2z^2\right)^3} + ... \tag{A-23}$$

For large values of R_2 (i.e. $R_2 >> (z_a + z)$), the ratio $b^2/4a^2$ is given by,

$$\frac{b^2}{4a^2} = \frac{k_1 \left(\frac{n^2 (z_a + z)}{R_2} + n \right)^2}{j \frac{2n^4}{R_2}}$$

$$\approx \frac{k_1 R_2}{j2n^2} \tag{A-24}$$

It is to be noted that for large R_2, $b/2a \rightarrow \infty$. Since we have previously assumed that k_1 is real, n^2 lies in the first quadrant and hence $1/jn^2$ lies in the third quadrant of the complex plane.

Thus we have $-3\pi/4 < \arg(b/2a) < 3\pi/4$. Now using the asymptotic expansion of the complementary error function as given in Eqn. A-23 for large b/2a we get the approximate value of V as,

$$V = \frac{2jk_2}{b}\frac{e^{jk_1R_2}}{R_2}\sqrt{\pi}\, b/2a\, e^{\frac{b^2}{4a^2}} erfc\left(b/2a\right)$$

$$\approx \frac{2jk_2}{b}\frac{e^{jk_1R_2}}{R_2}\left(1-\frac{jn^2}{k_1R_2}\right)$$

$$= -2\frac{e^{jk_1R_2}}{R_2}\left(1-\frac{jn^2}{k_1R_2}\right) \qquad \text{(A-25)}$$

REFERENCES

1. M. Abramowitz and I. Stegun, *Handbook of Mathematical Functions*. New York: Dover, 1965.
2. A. Banos, *Dipole Radiation in the presence of a conducting half-space*. Oxford: Pergamon Press, 1966.
3. L. M. Brekhovskikh, *Waves in Layered Media*, Academic Press, New York, 1960.
4. R. E. Collin, "Hertzian dipole radiating over a lossy earth or sea: some early and late 20th-century controversies," *IEEE Antennas and Propagation Magazine*, Vol. 46, Issue 2, April 2004, pp. 64-79.
5. R. E. Collin and F. J. Zucker, *Antenna Theory, Part I and II*, McGraw Hill Book Co., New York 1969.
6. A. R. Djordjevic, M. B. Bazdar, T. K. Sarkar, and R. F. Harrington, *AWAS Version 2.0: Analysis of Wire Antennas and Scatterers, Software and User's Manual*, Artech House, 2002.
7. H. von Hörschelman, Dissertation Munich 1911.
8. W. C. Jakes, *Microwave Mobile Communications.* New York: Wiley, 1974.
9. J. D. Kraus and R. J. Marhefka, *Antennas*, 3rd ed. New York: McGraw Hill, 2002.
10. J. C. Liberti, and T. S. Rappaport, Smart Antennas for Wireless Communications: IS-95 and Third Generation CDMA Applications. NJ, USA: Prentice Hall PTR, 1999.
11. E. K. Miller, A. J. Poggio, G. J. Burke and E. S. Selden, "Analysis of Wire Antennas in the Presence of a Conducting Half Space: Part I. The Vertical Antenna in Free Space", *Canadian J. of Physics*, Vol. 50, pp. 879-888, 1972.

12. E. K. Miller, A. J. Poggio, G. J. Burke and E. S. Selden, “Analysis of Wire Antennas in the Presence of a Conducting Half Space: Part II. The Horizontal Antenna in Free Space”, *Canadian J. of Physics*, Vol. 50, pp. 2614-2627, 1972.
13. K. A. Norton, “Propagation of radio waves over a plane earth,” *Nature* 135, pp. 954-955.
14. K. A. Norton, “The Propagation of Radio Waves over the surface of the earth and in the upper atmosphere”, *Proc. I.R.E.*, vol. 25, no. 9, Sept. 1937.
15. T. Okumura, E. Ohmori, and K. Fukuda, “Field strength and its variability in VHF and UHF land mobile service,” *Rev. Elect. Commun.Lab.*, vol. 16, no. 9–10, pp. 825–873, 1968.
16. T. K. Sarkar, *Analysis of Arbitrarily Oriented Thin Wire Antenna Arrays over Imperfect Ground Planes*. Dissertation Syracuse University 1975.
17. T. K. Sarkar, "Analysis of Arbitrarily Oriented Thin Wire Antennas over a Plane Imperfect Ground," *AEU*, Band 31, Heft 11, pp. 449-457, 1977.
18. T. K. Sarkar, S. Burintramart, N. Yilmazer, S. Hwang, Y. Zhang, A. De, and M. Salazar-Palma, “A Discussion about some of the principles/practices of wireless communication under a Maxwellian Framework,” *IEEE Trans. on Antennas and Propagation.*, Vol. 54, Issue 12, Dec. 2006, pp. 3727-3745.
19. T. K. Sarkar, S. Burintramart, N. Yilmazer, Y. Zhang, A. De, M. Salazar-Palma, M. Lagunas, E. Mokole and M. Wicks, “A Look at the Concept of Channel Capacity from a Maxwellian Viewpoint,” *IEEE Antennas and Propagation Magazine*, Vol. 50, No. 3, June 2008, pp. 21-50.

20. T. K. Sarkar, M. Salazar-Palma, and E. Mokole, *Physics of Multiantenna Systems and Broadband Processing*, John Wiley & Sons, New York, 2008.

21. T. K. Sarkar, M. C. Wicks, M. Salazar-Palma, and R. Bonneau, *Smart Antennas*, IEEE Press / John Wiley & Sons, 2003.

22. A. N. Sommerfeld, "Propagation of waves in wireless telegraphy," *Ann. Phys.* (Leipzig), 28, 1909, pp. 665-737.

23. A. N. Sommerfeld, "Propagation of waves in wireless telegraphy," *Ann. Phys.* (Leipzig), 81, 1926, pp. 1135-1153.

24. A. N. Sommerfeld, *Partial Differential Equations in Physics*. Vol.-VI New York: Academic Press, 1949.

25. G. Tyras, *Radiation and Propagation of Electromagnetic Waves*, Academic Press, New York 1960.

26. Balth.VanDerPol, "Theory of the reflection of the light from a point source by a finitely conducting flat mirror, with an application to radio telegraphy", *Physica 2*, pp 843-853, 1935.

27. G.N. Watson, *A Treatise in the theory of Bessel Functions*, University Press, Cambridge 1944.

28. W. Howard Wise, "Asymptotic dipole radiation formulas," *Bell Sys. Tech. Jour.*, vol. 8, pp 662-671; October (1929).